# *Seasonal and regional signatures of ENSO in upper tropospheric jet characteristics from reanalyses*

SPECIAL
MERRA-2
COLLECTION

# Seasonal and Regional Signatures of ENSO in Upper Tropospheric Jet Characteristics from Reanalyses

GLORIA L. MANNEY,[a,b] MICHAELA I. HEGGLIN,[c] AND ZACHARY D. LAWRENCE[d,e]

[a] *NorthWest Research Associates, Socorro, New Mexico*
[b] *New Mexico Institute of Mining and Technology, Socorro, New Mexico*
[c] *Department of Meteorology, University of Reading, Reading, United Kingdom*
[d] *Cooperative Institute for Research in Environmental Sciences, NOAA/Physical Sciences Laboratory, Boulder, Colorado*
[e] *NorthWest Research Associates, Boulder, Colorado*

(Manuscript received 9 December 2020, in final form 18 August 2021)

ABSTRACT: The relationship of upper tropospheric jet variability to El Niño–Southern Oscillation (ENSO) in reanalysis datasets is analyzed for 1979–2018, revealing robust regional and seasonal variability. Tropical jets associated with monsoons and the Walker circulation are weaker and the zonal mean subtropical jet shifts equatorward in both hemispheres during El Niño, consistent with previous findings. Regional and seasonal variations are analyzed separately for subtropical and polar jets. The subtropical jet shifts poleward during El Niño over the Northern Hemisphere (NH) eastern Pacific Ocean in December–February (DJF) and in some Southern Hemisphere (SH) regions in March–May and September–November (SON). Subtropical jet altitudes increase during El Niño, with significant changes in the zonal mean in the NH and during summer/autumn in the SH. Although zonal mean polar jet correlations with ENSO are rarely significant, robust regional/seasonal changes occur: The SH polar jet shifts equatorward during El Niño over Asia and the western Pacific in DJF and significantly poleward over the eastern Pacific in June–August and SON. During El Niño, polar jets are weaker in the Western Hemisphere and stronger in the Eastern Hemisphere, especially in the SH; conversely, subtropical jets are stronger in the Western Hemisphere and weaker in the Eastern Hemisphere during El Niño in winter and spring. These opposing changes, along with an anticorrelation between subtropical and polar jet wind speeds, reinforce subtropical–polar jet strength differences during El Niño and suggest ENSO-related covariability of the jets. ENSO-related jet latitude, altitude, and wind speed changes can reach 4°, 0.6 km, and 6 m $s^{-1}$, respectively, for the subtropical jets and 3°, 0.3 km, and 3 m $s^{-1}$, respectively, for the polar jets.

KEYWORDS: Atmosphere; Atmospheric circulation; Upper troposphere; ENSO; Jets; Interannual variability; Reanalysis data

## 1. Introduction

Jet streams in the upper troposphere (UT) are a prominent feature of the atmospheric circulation and play an essential role in variability in phenomena such as storm tracks, precipitation, and extreme weather events (Uccellini and Johnson 1979; Nakamura et al. 2004; Kolstad et al. 2010; Grotjahn et al. 2016; Harnik et al. 2016; Mann et al. 2017; Winters et al. 2019, and references therein). UT jets are sensitive to climate change and ozone loss, as well as to natural modes of variability (Lorenz and DeWeaver 2007; Scaife et al. 2008; McLandress et al. 2011; Hudson 2012; Lin et al. 2014, 2015; Waugh et al. 2015, 2018; Grise et al. 2018, and references therein). However, UT jets show complex patterns of seasonal and regional variability (Manney et al. 2014; Manney and Hegglin 2018; Spensberger and Spengler 2020, and references therein), which makes it difficult to disentangle their response to climate change (i.e., radiative forcing) from that to natural modes of variability.

The pattern of oscillating sea surface temperatures (SSTs) over the tropical ocean in the central and eastern Pacific known as El Niño–Southern Oscillation (ENSO) (with El Niño referring to the warm phase and La Niña to the cold phase of the oscillation) is one mode of natural variability that has been shown to influence the UT and stratospheric circulation (e.g., Yulaeva and Wallace 1994; Shapiro et al. 2001; Seager et al. 2003; L'Heureux and Thompson 2006; Calvo et al. 2010; Hall et al. 2015; Domeisen et al. 2019, and references therein). The UT jets are affected by ENSO via both tropospheric and stratospheric pathways, the former most directly influencing the subtropical jet, and the latter being critical to ENSO's influence on higher latitude jets (Hall et al. 2015, and references

Denotes content that is immediately available upon publication as open access.

Supplemental information related to this paper is available at the Journals Online website: https://doi.org/10.1175/JCLI-D-20-0947.s1.

*Corresponding author*: Gloria L. Manney, manney@nwra.com

DOI: 10.1175/JCLI-D-20-0947.1

therein). In this paper, we will focus on comprehensively characterizing and quantifying the relationship of ENSO to UT jet variability.

Knowledge of this relationship is important because changes in UT jet streams are linked to changing regional weather and climate patterns (Lucas et al. 2014; Harnik et al. 2016; Mann et al. 2017; Winters et al. 2019, and references therein). Tropical, subtropical, and extratropical UT jets have been linked to rainfall changes in the tropics (e.g., Hulme and Tosdevin 1989; Bollasina et al. 2014; Kelly et al. 2018; RavindraBabu et al. 2019), subtropics (e.g., Price et al. 1998; Raible et al. 2004; Lucas et al. 2014; Huang et al. 2015; Xie et al. 2015), and midlatitudes (e.g., Kang et al. 2011; Thompson et al. 2011; Delworth and Zeng 2014; Bai et al. 2016; Zhao et al. 2018). These rainfall changes are often correlated with ENSO phases. Likewise, circulation changes reflected in UT subtropical and lower-tropospheric or UT higher-latitude jet variations have been linked to both ENSO influences and to extreme weather events over North America (e.g., Garfinkel and Hartmann 2008; Wettstein and Wallace 2010; Wang et al. 2014; Hartmann 2015; Yu and Zhang 2015; Martineau et al. 2021) and Europe (e.g., Schubert et al. 2011; Santos et al. 2013; K. Zhang et al. 2019). Characterizing how the UT jets vary with ENSO can thus lead to improving our understanding of and ability to predict links between SST anomalies, UT jet variations, and high-impact weather events.

Until recently most studies of variability and climate-related changes in the UT subtropical jet were of zonal means or averages in broad regions (Lorenz and DeWeaver 2007; Strong and Davis 2007, 2008; Lucas et al. 2014; Staten et al. 2016; Maher et al. 2020, and references therein). Several studies have shown differing jet latitude trends and/or relationships to natural modes of variability in some regions and seasons (e.g., Lucas et al. 2012; Peña-Ortiz et al. 2013; Lucas and Nguyen 2015; Manney and Hegglin 2018). Spensberger and Spengler (2020) recently showed qualitatively some regional characteristics of ENSO-related changes in the UT jets, suggesting an equatorward shift of the subtropical jet during El Niño in some regions of the winter hemispheres. Gillett et al. (2021) reported an equatorward shift of the wintertime Southern Hemisphere (SH) subtropical jet during El Niño in the Indo-Pacific longitude region where it is strongest and most zonal; they also suggested links to "polar jet" variability but defined the polar jet using low-level winds.

To our knowledge, no comprehensive study has quantified the relationships of ENSO to the UT jets over the full range of regional and seasonal variability. In this paper, we analyze products from the Jet and Tropopause Products for Analysis and Characterization (JETPAC) software package [developed by Manney et al. (2011) and Manney and Hegglin (2018)] to characterize the relationships of UT jets to ENSO from 1979 through 2018 in reanalysis datasets as a function of region and season. Our analysis characterizes these relationships for the subtropical (largely radiatively driven) and polar (largely eddy driven) UT jets [for taxonomy, see, e.g., Held et al. (2002) and Lee and Kim (2003)] separately. This separation, often neglected in earlier studies, is key given that these jets have shown distinct, sometimes opposite, long-term behavior in different regions and seasons (see, e.g., Manney and Hegglin 2018, and references therein). Section 2 describes the datasets and methods used; section 3b compares geographic patterns for El Niño and La Niña periods; section 3c discusses correlations between ENSO and jet characteristics by region and season; section 3e provides discussion and synthesis of these results. Our conclusions are given in section 4.

## 2. Data and methods

### a. Reanalysis datasets

We use JETPAC (see section 2b; Manney et al. 2011) to calculate jet core latitude, altitude, and wind speed for polar and subtropical UT jets from three modern "full-input" reanalyses (those that assimilate a full suite of satellite and conventional measurements; see, e.g., Fujiwara et al. 2017) that have been shown to be suitable for upper-troposphere–lower-stratosphere (UTLS) studies (e.g., Long et al. 2017; Manney et al. 2017; Xian and Homeyer 2019; Homeyer et al. 2021): NASA's Global Modeling and Assimilation Office's (GMAO) Modern-Era Retrospective Analysis for Research and Applications, version 2 (MERRA-2) (Gelaro et al. 2017); ECMWF's ERA-Interim (Dee et al. 2011); and the JMA's 55-year reanalysis (JRA-55) (Ebita et al. 2011; Kobayashi et al. 2015). Because characteristics (such as jet core locations) that are identified by analysis of patterns in global or regional fields cannot be observed directly, reanalyses from modern data assimilation systems are our best tools for studying such phenomena. Numerous studies highlight the importance of comparing results among reanalyses for UTLS studies (e.g., Manney et al. 2017; Manney and Hegglin 2018; Xian and Homeyer 2019; Tegtmeier et al. 2020; Wright et al. 2020; Homeyer et al. 2021; Tegtmeier et al. 2021).

Table 1 summarizes the information about the reanalyses products studied herein that is most relevant to this paper. One feature of MERRA-2 (Gelaro et al. 2017) that is different from the other reanalyses is that the assimilation system uses an Incremental Analysis Update (IAU) (Bloom et al. 1996) to constrain the analyses. Both "Analyzed" (prior to IAU) and "Assimilated" (after IAU) data collections are provided by the Global Modeling and Assimilation Office (GMAO). We use the Assimilated data collection (GMAO 2015), as recommended by GMAO (see, e.g., https://gmao.gsfc.nasa.gov/reanalysis/MERRA-2/docs/ANAvsASM.pdf; Fujiwara et al. 2017). The year 1979 is considered to be a spinup year for MERRA-2, and thus those data are not in the public record; we use data for December 1979 here in the seasonal calculations for December–February (DJF). The models, assimilation systems, and data inputs for the reanalyses are described in detail by Fujiwara et al. (2017).

Calculations are done using daily 1200 UTC fields from each reanalysis dataset. Manney et al. (2017) describe sensitivity tests showing that using a different hour of the day (e.g., 0000 UTC vs 1200 UTC), or using all available hours in the day, does not notably affect the results, so a single hour is used for computational efficiency. The reanalysis fields are used on their native model levels and near their native horizontal resolution, as indicated in Table 1 (for spectral models, this means a longitude–latitude grid with spacing commensurate with the

TABLE 1. Reanalysis product summary information.

| Reanalysis | Grid | No. of levels | Model top height (hPa) | UTLS approx. level spacing (km) | Reference |
|---|---|---|---|---|---|
| MERRA-2 | 0.625° × 0.5° | 72 | 0.01 | 1.2 | Gelaro et al. (2017) |
| ERA-Interim | 0.75° × 0.75° | 60 | 0.1 | 1 | Dee et al. (2011) |
| JRA-55 | 0.56° × 0.56°[a] | 60 | 0.1 | 1 | Kobayashi et al. (2015) |

[a] Approximately; these fields are provided on a Gaussian grid.

Gaussian grid implied by the spectral resolution of the model). The vertical resolution in the UTLS for each of these reanalyses is near 1 km, slightly higher for MERRA-2 than for the other reanalyses used herein [see Table 1 herein and Fujiwara et al. (2017, their Fig. 3)]. Vertical resolution and spacing are critical to representation of UT jets and tropopauses (e.g., Manney et al. 2017).

### b. Methods

#### 1) JETPAC

Upper-tropospheric jet characterization using JETPAC is described in Manney et al. (2011, 2014, 2017) and Manney and Hegglin (2018). Briefly, JETPAC identifies UT jets in latitude/height slices of three-dimensional (3D) gridded meteorological data as wind speed maxima greater than 40 m s$^{-1}$ between 400 and 100 hPa, with the jet region defined where the wind speed remains above 30 m s$^{-1}$; when multiple such maxima occur in the same jet region, they are identified as separate jets cores if either the latitude difference or the wind speed decrease between them is larger than a threshold value [see Manney et al. (2011) for further details and demonstration of insensitivity to reasonable ranges for these thresholds].

The subtropical jet is defined as the lowest latitude westerly jet for which the primary temperature gradient (World Meteorological Organization) tropopause altitude at its equatorward edge is at least 13 km and the tropopause altitude drops by at least 2 km from the equatorward to the poleward edge of the jet; it is thus identified in a physically meaningful way as the jet across which the ''tropopause break'' occurs. The polar jet is taken to be the strongest westerly jet poleward of the subtropical jet (or 40° latitude if there is no subtropical jet). While the criterion for identifying the polar jet is just one possible choice (e.g., one might include all westerly jets poleward of the subtropical jet at each longitude), as tested by and discussed in Manney and Hegglin (2018), our results are insensitive to the details of the polar jet definition once the subtropical jet is defined. These criteria provide physically meaningful definitions that distinguish the jets that most closely approximate the idealized ''radiatively driven'' (the subtropical jet) and ''eddy-driven'' (the polar jet) types; in reality, there is a spectrum of jets that often have characteristics that are a hybrid between the two (e.g., Lee and Kim 2003; Manney et al. 2014).

Jet core location frequency distributions are calculated in 3° latitude by 6° longitude bins and are normalized by the number of jets that would ''fill'' each bin if one were identified at every longitude in that bin. Frequency results represent the jet frequency as a percentage of the number of jets it would be possible to have if there was a jet at every longitude in the bin on every day. Because the JRA-55 Gaussian grid on which that dataset is provided does not have an integer number of grid points in each bin, the JRA-55 data are interpolated to a 0.5° × 0.5° latitude × longitude grid before computing frequency distributions (the native grid is used for the other analyses in this paper). See Manney et al. (2014, 2017) for further details on binning and normalization.

#### 2) ANALYSIS

Relationships with ENSO are assessed qualitatively using composites for extremes of and correlations with the multivariate ENSO index, version 2 (MEIv2; T. Zhang et al. 2019), which is an adaptation of the widely used MEI described by Wolter and Timlin (2011). (All calculations in this paper were also done using the MEI, with very similar results.)

Figures S1 and S2 in the online supplemental material show results testing sensitivity to comparing El Niño with La Niña composites versus comparing each with neutral conditions, and to the threshold MEIv2 magnitudes chosen to represent El Niño and La Niña conditions. The anomalies from climatology and neutral states [Fig. S1 shows September–November (SON); other seasons are similar] are qualitatively very similar to those for the El Niño/La Niña anomalies; we thus show the anomalies as El Niño–La Niña differences hereinafter. Since numerous thresholds have been used in the literature, we tested thresholds of 0.94, 0.7, and 0.56 for MEIv2 magnitude. Figure S2 shows that all three choices give similar results, and we use 0.94 for compositing hereinafter. Because the composites are based on a small sample of El Niño and La Niña years, and depend on choosing subjective thresholds, they provide a qualitative overview of the patterns of jet differences between El Niño and La Niña conditions.

To quantify the results, we study correlations of subtropical and polar jet latitude, altitude, and wind speed with the MEIv2. Jet time series are constructed following Manney and Hegglin (2018): Latitude, altitude, and wind speed of the subtropical and polar jets cores were calculated at each longitude of the reanalysis grids for each day using 1200 UTC fields; these are then averaged for month and season [DJF, March–May (MAM), June–August (JJA), and SON], zonally and in 20° longitude bins (from 180°–160°W to 160°E–180°). The 40-yr (from 1979 to 2018) times series for each of these seasons and longitude regions is then correlated with the MEIv2 index time series for the corresponding month or season. Both MEIv2 and jet diagnostic time series are detrended before calculating correlations.

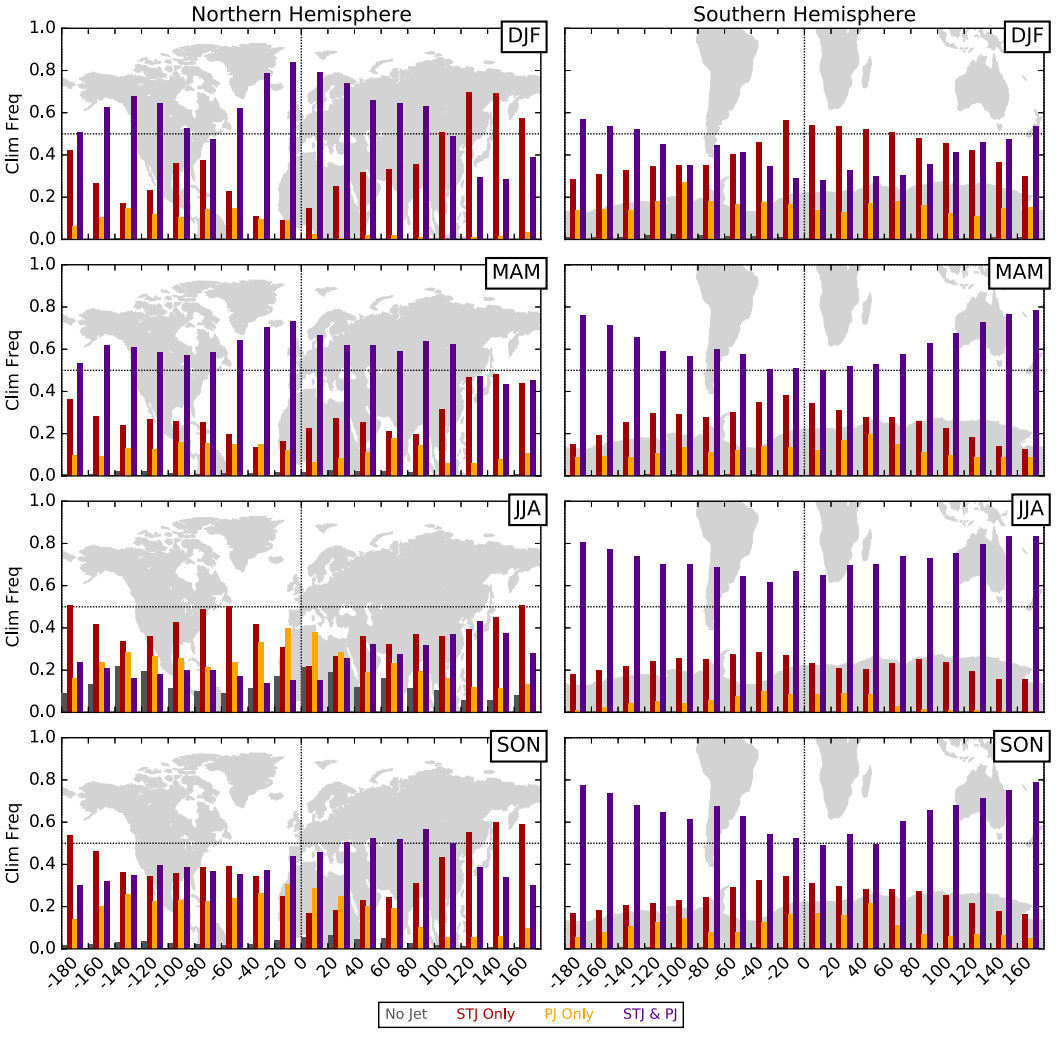


FIG. 1. Climatological (1980–2018) relative occurrence frequencies in 20° longitude bins for each season and hemisphere of no jets (dark gray), subtropical jet only (red), polar jet only (orange), and both subtropical and polar jets (purple). Plots are normalized so that the total of each set of bars is 1; that is, each bar is mutually exclusive and represents the fraction of locations/times in that bin when that specific combination of jets occurs. Data are from the MERRA-2 reanalysis; Figs. S1 and S2 in the online supplemental material show the same plot for the ERA-Interim and JRA-55 reanalyses, respectively.

The results of the correlation analysis are presented by showing the slope of the linear fit multiplied by the difference in MEIV2 between the El Niño and La Niña thresholds; these values thus represent the change in the value of the jet diagnostic that would occur if conditions changed from the weakest La Niña to the weakest El Niño.

The statistical significance of the correlations is assessed using simple bootstrap resampling (e.g., Efron and Tibshirani 1993) to construct 100 000 artificial time series based on the input data time series. This was used to construct 95% and 99% confidence intervals for the correlations. Since our results are based on monthly and seasonal means that can be reasonably assumed to be independent from year to year, more sophisticated bootstrapping methods are unnecessary. We have, however, done the calculations using fixed block and "stationary" (Politis and Romano 1994) bootstrapping, with results very similar to those shown here. The significance of El Niño/La Niña composite differences was estimated using a permutation analysis (e.g., Wilks 2011), wherein the sequence of years was shuffled randomly to get 50 000 instances, and then the "El Niño" and "La Niña" years were selected from these to obtain a confidence interval [similar to the procedure used by Manney and Hegglin (2018) for trend significance].

## 3. Results

### a. *Relevant climatological jet relationships*

Figure 1 illustrates the climatological occurrence frequency of subtropical and polar jets identified as described above

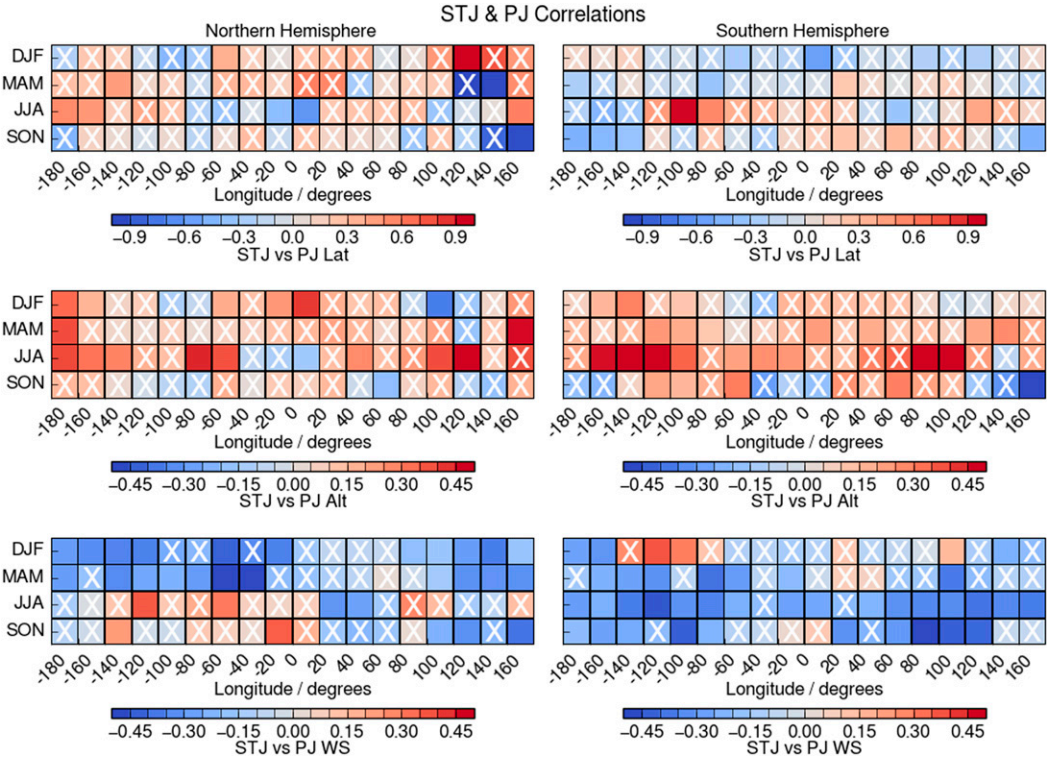


FIG. 2. Summary matrices for correlations of subtropical jet with polar jet (top) latitude, (middle) altitude, and (bottom) wind speed. Color fill shows the value of the expected change in the polar jet if the subtropical jet value increases by one unit (degree, kilometer, or meter per second for latitude, altitude, or wind speed, respectively). Absolute value of latitude is used, so positive values represent poleward shifts in both hemispheres. Correlation coefficients for bins with a white X were not significant at the 95% confidence levels as based on the bootstrapping analyses (see text). Values are from the reanalysis with the maximum change.

relative to the total jet occurrence frequency for each season. We show the fraction of each longitude bin and season with no jet, only a subtropical jet, only a polar jet, or both subtropical and polar jets. Thus, each bar in a group of four represents a mutually exclusive state, with the sum for each region/season equal to 1 (i.e., normalized by the total number of jets in that bin). The total fraction of each bin with a subtropical or polar jet is thus the sum of the ''both'' bar and the subtropical or polar jet bar, respectively. (Figures S3 and S4 in the online supplemental material show that these relationships are very similar in the other reanalyses used herein.) In both hemispheres, both jets are most often present at the same time and in the same longitude bin in winter and least often present at the same time and in the same longitude bin in summer, consistent (when the subtropical only and both jets bars are summed) with the climatological spectrum of jets showing strongest and most persistent subtropical jets in winter (e.g., Manney et al. 2014). At least one jet is nearly always present except in boreal summer when there is no jet identified in some regions up to about 20% of the time. A subtropical jet alone is the prevalent mode in most regions during summer in both hemispheres [more so in the Northern Hemisphere (NH) than in the SH]. Although the equinox seasons in the SH show almost identical frequencies of the different modes in autumn and spring, in the NH the spring frequencies are reminiscent of those found in winter and the autumn frequencies are reminiscent of those found in summer. A notable exception to this overall pattern is over the NH western Pacific, where the subtropical jet only mode dominates throughout the year. Both subtropical and polar jets are present 60%–80% of the time in SH winter, and 50%–80% of the time in SH autumn and spring, with the lower frequencies over the Atlantic and Africa. Figure S5 in the online supplemental material illustrates for MAM (the season with the largest differences between El Niño and La Niña) that the relative occurrence frequencies of the different jet categories shown in Fig. 1 do not change notably from climatology for El Niño or La Niña conditions.

Figure 2 summarizes correlations between subtropical and polar jet latitudes, altitudes, and wind speeds. Subtropical and polar jet latitudes tend to be weakly positively correlated in the NH and weakly negatively correlated in the SH, but those correlations are rarely significant. Significant positive correlations of subtropical and polar jet altitude are seen in a few regions and seasons, with the largest region of correlations in JJA in the SH, and a smaller region in the NH near the date line in DJF, MAM, and JJA. Correlations between subtropical jet and polar jet wind speeds are usually negative, and they are significant over most regions in winter and spring (DJF and

MAM in the NH; JJA and SON in the SH.) Only very isolated regions show significant positive wind speed correlations, in JJA and SON in the NH and in DJF in the SH. Comparison with Fig. 1 shows that the strongest negative correlations in winter/spring are in regions where both jets tend to be present (although not all regions commonly having both jets show strong correlations). While previous studies are not directly comparable with ours, in particular because of very different definitions of the polar (i.e., eddy driven) jet, several have shown an anticorrelation between subtropical and eddy-driven jet strength (e.g., Lee and Kim 2003). In addition, Gillett et al. (2021) showed that these relationships may be masked by regional variations in a zonal-mean view.

Changes in different jet characteristics (latitude, altitude, and wind speed) with ENSO may not show the same relationships in different regions/seasons but may be linked by the relationships between those characteristics. As shown in previous work (e.g., Lorenz and DeWeaver 2007; Manney and Hegglin 2018; Melamed-Turkish et al. 2018; also see Fig. S6 in the online supplemental material), the altitude of both subtropical and polar jets nearly always decreases with a poleward shift of that jet. Subtropical jet wind speeds nearly always increase as that jet moves poleward; conversely, polar jet wind speeds typically decrease as that jet moves poleward (Fig. S6). The thermal wind relationship predicts increasing wind speed with decreasing pressure (and thus increasing altitude) for a given meridional temperature gradient, which is consistent with the relationship seen for the polar jet and with some previously reported regional jet relationships (see, e.g., Melamed-Turkish et al. 2018, and references therein). They also noted that changes in baroclinicity related to wave forcing may contribute to a poleward shift of the polar jet as its speed increases, and several studies have shown a similar result for the eddy-driven jet in the lower troposphere (e.g., Chen and Held 2007; Ceppi and Hartmann 2013; Gillett et al. 2021). The opposite relationship for the subtropical jet appears consistent with that jet being sustained against eddy stresses by strong poleward angular momentum flux from the tropics; again, the varying contributions of eddy driving to both jets (e.g., Lee and Kim 2003) may add complexity to these relationships. The difference in relationships of latitude (and hence altitude) with wind speed for subtropical versus polar jets supports the ability of our methods to distinguish jets with different primary driving mechanisms.

These climatological relationships between the subtropical and polar jets, and between different characteristics of each jet, are helpful to inform our analysis in the following sections of ENSO-related changes in these characteristics. They will be discussed further in section 3e.

### b. Jet distributions by ENSO phase

Figures 3–6 show composite latitude–altitude cross sections and maps of jet core climatological frequency distributions and jet core wind speeds, and the differences between those distributions for El Niño and La Niña conditions from the MERRA-2 reanalysis. The difference plots show results for all jets (i.e., all tropical and extratropical jets, both easterly and westerly), subtropical jets only, and polar jets only, respectively. (Figures S7 and S8 in the online supplemental material show the corresponding climatologies and all jet differences for ERA-Interim and JRA-55 for the solstice seasons, demonstrating close agreement among the reanalyses.) Changes in jet core frequency and jet core wind speed are related because the existence of a jet core is determined by wind speed criteria, and because stronger jets show less variability (e.g., Woollings et al. 2018). This does not imply a one-to-one relationship, especially in composites that may combine effects of position and strength changes in multiple jets. However, many of the most robust patterns of El Niño/La Niña differences are reflected in both frequency and jet core wind speed.

The solstice seasons are shown in Figs. 3 and 4. Both frequency and wind speed anomalies are weaker in DJF than in JJA in both hemispheres. Broad areas of positive SH wind speed anomalies in the subtropics and higher latitudes in JJA suggest that El Niño is associated with stronger SH extratropical jets; the subtropical jet only composites suggest that these changes are primarily related to stronger subtropical jets when that jet is at lower latitude. A dipole pattern in the zonal mean with positive anomalies equatorward of and above negative anomalies indicates an equatorward or poleward shift of the subtropical jets during El Niño or La Niña, respectively, in JJA, and in the SH in DJF. The NH pattern is less clear in DJF and could instead represent a widening and weakening of the subtropical jet under El Niño conditions. The weaker NH shift in the latitude/altitude sections in JJA reflects strong regional variations in the subtropical jet latitude as it shifts northward around the ASM anticyclone (e.g., Schiemann et al. 2009; Manney et al. 2014), which obscures differences in the zonal mean view. The zonal-mean equatorward shift during El Niño reflects changes in the longitude region where the subtropical jet is strongest and most zonally oriented, which spans the Eastern Hemisphere in both seasons and both hemispheres, but also extends over the eastern Pacific in the SH in JJA. Similar, but more diffuse, patterns are seen in the wind speed anomalies. These results are consistent with a previously reported equatorward shift of surface westerlies during El Niño (e.g., Chen et al. 2008), as well as zonal mean and regional shifts in the winter subtropical jets in both hemispheres (e.g., Seager et al. 2003; L'Heureux and Thompson 2006; Spensberger and Spengler 2020; Gillett et al. 2021). A NH equatorward subtropical jet shift in JJA for El Niño conditions from about 90°E–180° [in the Asian summer monsoon (ASM) region] is consistent with previous work showing a positive correlation between subtropical jet latitude and ASM anticyclone centroid latitude, and a negative correlation of ASM anticyclone centroid latitude with MEI (Manney et al. 2021).

Tropical jets are most prevalent during the solstice seasons shown in Figs. 3 and 4. Occurrence frequencies of the tropical easterly jet associated with the ASM anticyclone (which stretches from about 30° to 130°E and from 20° to 40°N in JJA; e.g., Manney et al. 2021) (Fig. 4) are lower under El Niño conditions. The tropical westerly jet just south of the equator in DJF and JJA (Figs. 3 and 4; also seen in SON; see below) (near 140° to 90°W; Manney et al. 2014) is also weaker during El Niño. This jet is associated with the Walker circulation (which results in upper-level westerlies downstream of the upper-level

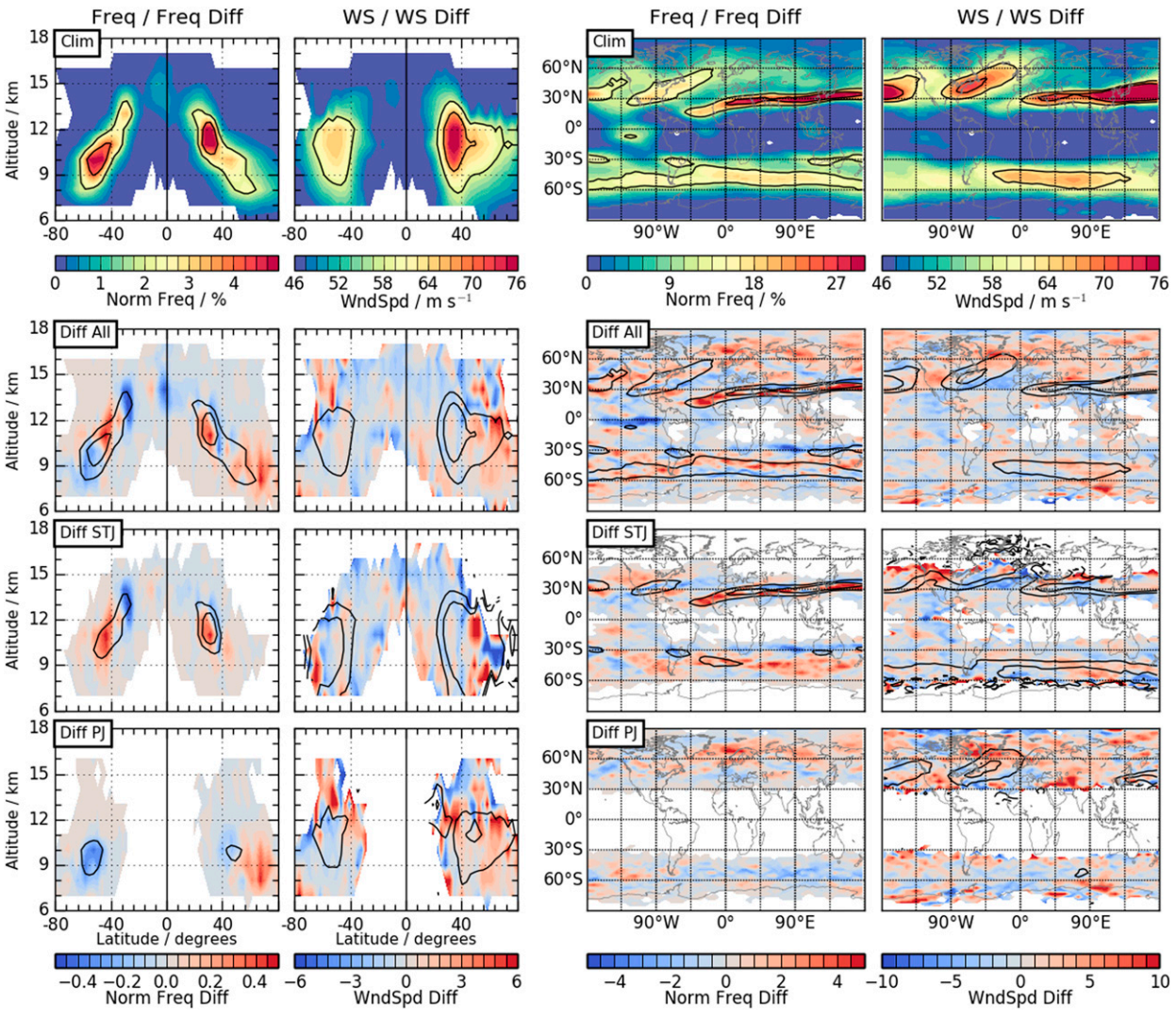


FIG. 3. Climatological (1979–2018) UT (top) jet frequency distributions (first and third columns) and jet core wind speeds (second and fourth columns) and the difference between the distributions for El Niño and La Niña years for (top middle) all jets, (bottom middle) subtropical jets only, and (bottom) polar jets only, from the MERRA-2 reanalysis for DJF for (left),(left center) latitude–altitude cross sections and (right center),(right) maps at the jet core altitude. Frequency distributions are calculated in 6° longitude by 3° latitude bins for the maps and 3° latitude by 1-km altitude bins for the cross sections and are normalized as described in the text (section 2b). Climatological frequency and wind speed contours for the corresponding jet type (all, subtropical, or polar) are overlaid on the difference panels. The ENSO threshold is MEIv2 magnitude greater than 0.94. Note that the El Niño–La Niña differences in the frequency distributions are the absolute (as opposed to percent) differences between two fields that are expressed as a percent in the climatological plots. DJF composites are based on 6 El Niño and 7 La Niña years.

easterlies associated with the Australian monsoon). Figures 3 and 4 show that zonal mean tropical jet frequencies and wind speeds decrease under El Niño conditions in both solstice seasons. These results are consistent with previous work showing that La Niña is associated with stronger tropical circulations, including the ASM circulation, Walker circulation, and the ''westerly ducts'' (which allow propagation of Rossby waves across the equator) (Julian and Chervin 1978; Horinouchi et al. 2000; Waugh and Polvani 2000; Tanaka et al. 2004; Shaman and Tziperman 2007; Bayr et al. 2014; Spensberger and Spengler 2020, and references therein).

The patterns of ENSO-related changes in the higher-latitude jets are more difficult to interpret. In JJA (Fig. 4) in the SH, anomalies in the region where the climatological subtropical jet spirals in to join the polar jet (between ~90°W and 45°E; e.g., Williams et al. 2007; Manney et al. 2014) appear consistent with a poleward shift of that jet during El Niño conditions; the subtropical jet only frequency changes indicate that this pattern is mostly associated with changes in that jet. The SH polar jet only differences in Fig. 3 indicate that high anomalies near 50°S in DJF in the zonal mean arise from more frequent polar jet occurrence at most longitudes. In JJA,

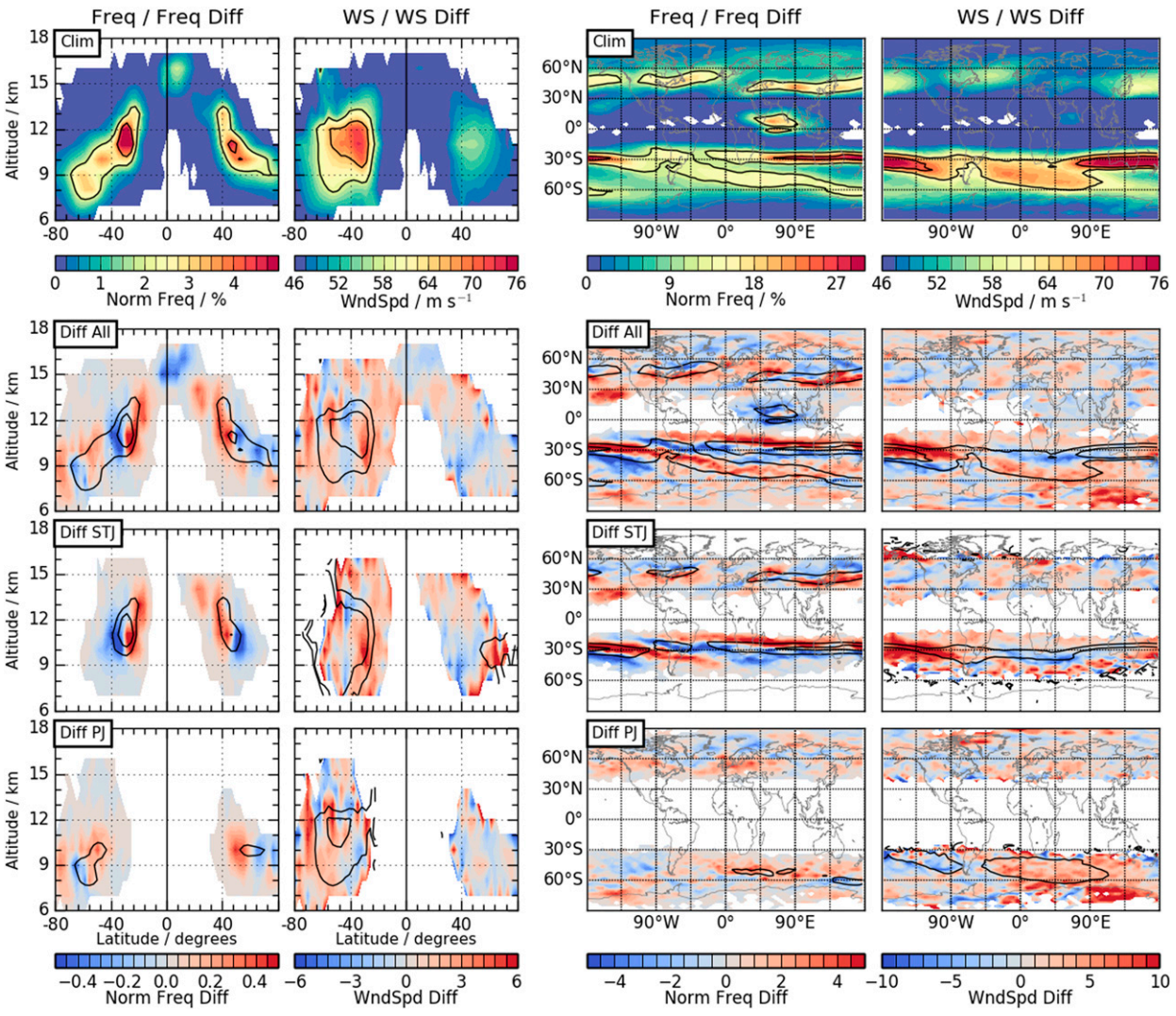


FIG. 4. As in Fig. 3, but for JJA. JJA composites are based on 5 El Niño and 4 La Niña years.

the patterns of polar jet only frequencies in the South Pacific (from about 130°E through 180° to 45°W) indicate an increase in jet frequency and wind speed in the Western Hemisphere during El Niño, along with corresponding decreases in the Eastern Hemisphere. A similar though weaker pattern is seen in the distributions for all jets. Weak wind speed anomalies in the altitude–latitude cross sections are consistent with the averaging of this pattern.

In both equinox seasons (Figs. 5 and 6), most jet changes are similar in character to those in JJA in both hemispheres. The subtropical jet shifts equatorward during El Niño in the latitude–altitude view. In the NH, such a shift is apparently nearly globally in MAM, and everywhere except over about 90°W–0° in SON. In both seasons, the SH subtropical jet shifts poleward during El Niño in the region where it spirals in to meet the polar jet, as was seen in JJA. The anomalies for all jets, confirmed by those for the polar jet only, in the South Pacific (from about 130°E through 180° to 45°W) indicate that the polar jet shifts poleward during El Niño in both MAM and SON, similar to its behavior in JJA. A weaker poleward shift is seen in both seasons over North America, the Atlantic, and Asia, and in SON over the western North Pacific. However, the complexity of the jet distributions in these regions and the contrasting patterns in the polar jet only composites preclude precise attribution of the origins of these patterns. More prevalent negative and positive SH wind speed changes over the Western and Eastern Hemispheres, respectively, during both equinoxes are largely related to changes in polar jet wind speed, and similar changes are seen in the NH in SON. In MAM, all of the extratropical jets show an upward shift during El Niño; in the SH the poleward part of this appears to be linked to an increase in polar jet frequency.

The above analysis of composites is limited by the small sample size (i.e., 4–7 El Niño/La Niña years depending on season and phase), the use of subjective ENSO thresholds, and

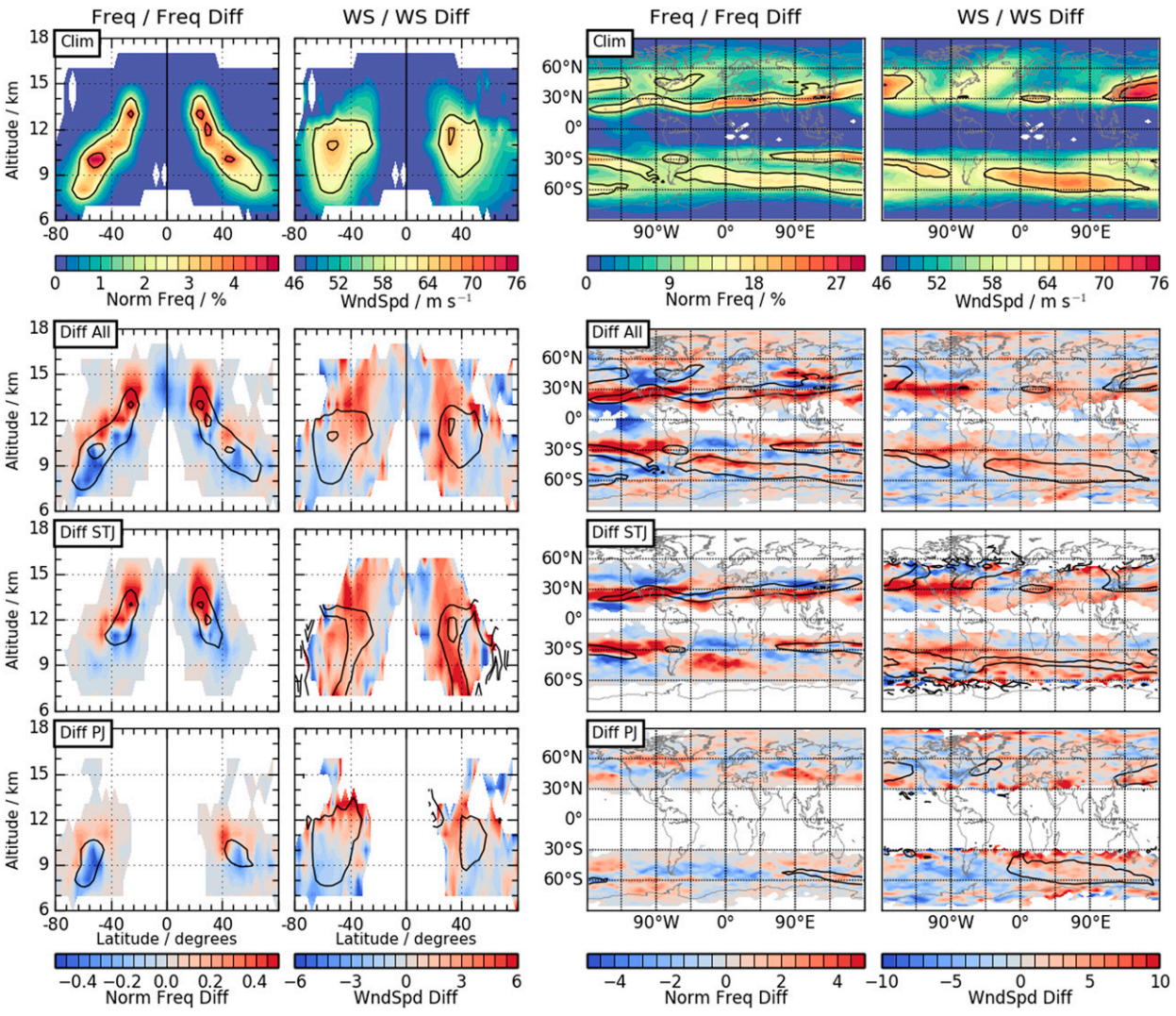


FIG. 5. As in Fig. 3, but for MAM. MAM composites are based on 6 El Niño and 6 La Niña years.

difficulty in interpretation engendered by the vast regional and seasonal variability in the jet distributions. It is thus not too surprising that the significance of the ENSO-related anomalies shown above [see section 2b(2)] exceeds the 90% confidence level in fairly limited regions (Fig. S9 in the online supplemental material). The regions/seasons where it does are typically those noted above with the clearest anomaly patterns: These include the large changes over the eastern Pacific and Americas in MAM in both hemispheres and JJA and SON in the SH, as well as frequency changes in MAM and SON over parts of Europe and Asia. The most significant changes in the zonal means include the tropical jets; large changes in both subtropical and higher-latitude jets in the SH in MAM, JJA, and SON; and subtropical jets changes in the NH in MAM and SON. Several regions of weaker wind speeds during El Niño in both hemispheres in MAM and in the SH in JJA and SON are also significant.

Despite these limitations, the above composite analysis confirms that our method of distinguishing subtropical and polar jets captures the full range of subtropical and extratropical variability associated with ENSO changes and also demonstrates substantial—albeit complex—variations of those jets with ENSO. Thus, we now turn to correlations of the MEIv2 index with subtropical and polar jet latitude, altitude, and wind speed for a more detailed and quantitative view of ENSO-related seasonal and regional jet variability.

### c. *Jet–ENSO correlations: Zonal mean view*

Figures 7 and 8 show changes in jet latitude, altitude, and wind speed with MEIv2 for the three reanalyses averaged over all longitudes as a function of month and season.

In the global view, the subtropical jet (Fig. 7) shows a robust equatorward and upward shift during El Niño periods. The results for the three reanalyses agree very closely in all cases. Seasonal (rightmost four sets of bars) latitude changes in the NH are significant in all cases except for MERRA-2 in DJF; in the SH, seasonal changes are significant except for MERRA-2

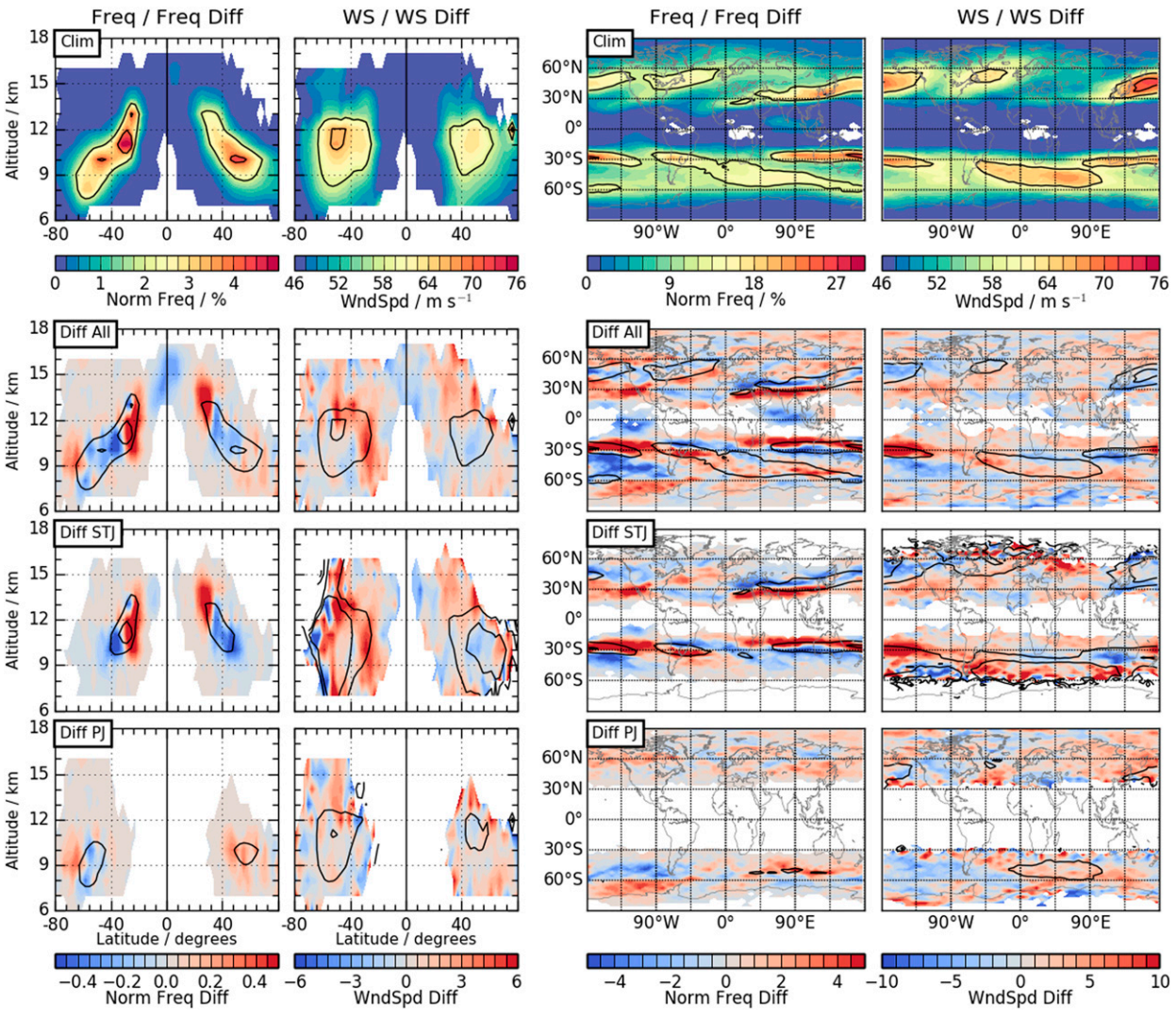


FIG. 6. As in Fig. 3, but for SON. SON composites are based on 6 El Niño and 7 La Niña years.

in MAM. Seasonal altitude changes in Fig. 7 are significant in all seasons and reanalyses in the NH, and in DJF and MAM in the SH, consistent with the patterns of altitude increases during El Niño shown in section 3b that are stronger in the NH and weaker in the SH during these seasons. These seasonal results arise from significant subtropical jet latitude and altitude shifts in the NH in most months, significant SH latitude shifts in January–April and September, and significant SH altitude shifts in January–May and November–December. The monthly jet shifts that are not significant are negative for latitude except in May in the SH, and always positive for altitude.

Subtropical jet wind speed changes with ENSO are less consistent, but significantly stronger wind speeds during El Niño (positive values) are seen in the NH in January–April, DJF, and MAM. October and SON show significantly weaker NH winds during El Niño. In the SH, the wind speed changes always indicate increases with El Niño (positive values) and are significant in June, October–November, MAM, and SON.

Changes of polar jet characteristics with MEIv2 (Fig. 8) are much less significant and more variable than those for the subtropical jet, likely because of the greater complexity associated with more indirect (including stratospheric) pathways of tropical–extratropical teleconnections for ENSO influence on higher latitudes (e.g., Hall et al. 2015; Stan et al. 2017; Domeisen et al. 2019, and references therein). Robust (i.e., significant in all reanalyses at the 95% confidence level) equatorward polar jet shifts during El Niño are seen only in the SH in December. Byrne et al. (2017, 2019) showed that the SH lower tropospheric zonal-mean eddy-driven jet was affected by ENSO primarily via the stratospheric polar vortex, and only during December, consistent with our SH result. Robust altitude increases during El Niño (positive changes) are seen in the NH in April and MAM, and in the SH in January, March, and MAM. In the NH, there is a robust signature of weaker winds during El Niño in March. In the SH, robust strengthening of the polar jet is seen in September and robust weakening is seen in DJF.

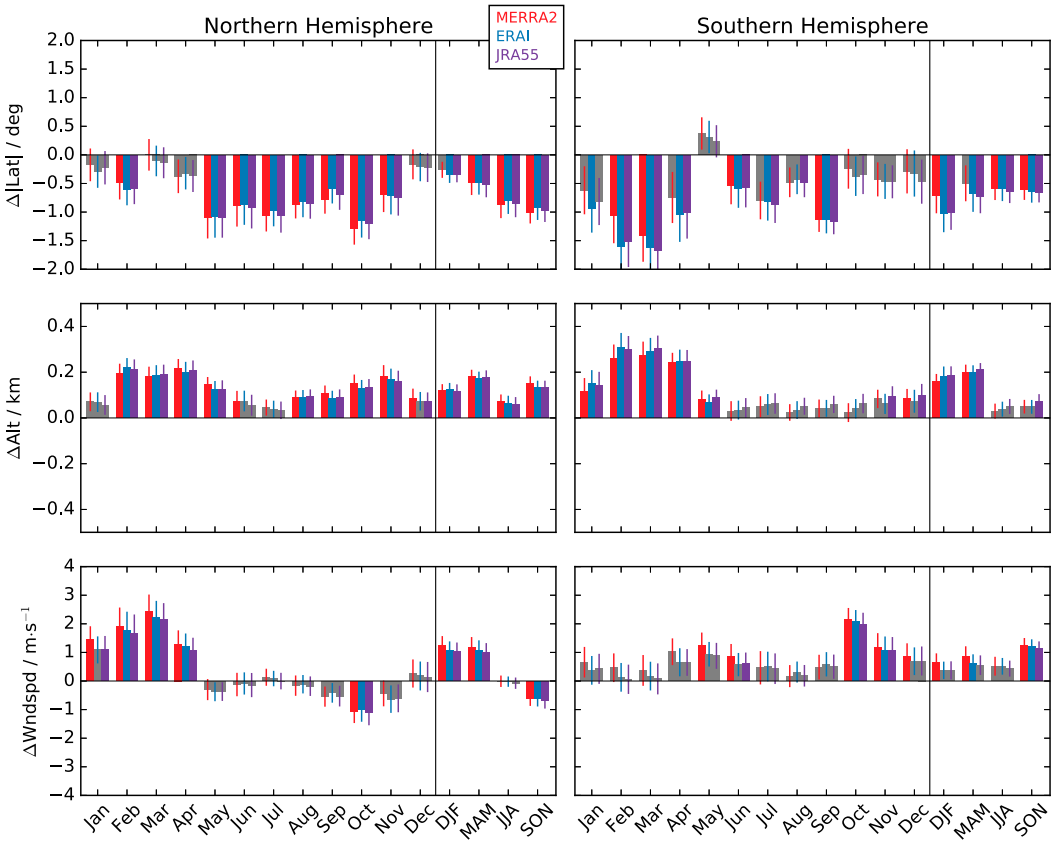


FIG. 7. Summary of monthly and seasonal 1979–2018 subtropical jet change with the MEIv2 ENSO index for jet core (top) latitude, (middle) altitude, and (bottom) wind speed for MERRA-2 (red; left of triplet), ERA-Interim (blue; center of triplet), and JRA-55 (purple; right of triplet). Bars represent the expected difference if conditions changed from the weakest La Niña to the weakest El Niño. Bars are shown in reanalysis colors when the correlations are significant at least at the 95% confidence level using a bootstrap analysis (see section 2b). Whiskers show the maximum among the reanalyses of the standard error of the linear fit. Absolute value of latitude is used in the SH so that positive or negative values always indicate that El Niño or La Niña, respectively, is associated with a more poleward jet position.

### *d. Jet–ENSO correlations: Regional variations*

Because of strong regional variability (e.g., Figs. 3–6), regionally resolved correlations provide further insight into these relationships. Figures 9 and 10 show these changes in 20° longitude bands in each season for subtropical and polar jets, respectively. Because consistently good agreement among the three reanalyses has been demonstrated, only the range of reanalysis differences is shown in these figures.

Consistently strong subtropical jet latitude decreases during El Niño (Fig. 9) are limited to about 180°–100°W and 20°–140°E in all seasons and both NH and SH; furthermore, not all seasons show large or significant changes over all of these regions. SH jet latitude in MAM is significantly lower during El Niño over about 180°–80°W, and significantly higher during El Niño over about 40°W–20°E. Poleward SH subtropical jet shifts are also seen in SON over 60°W–20°E. In DJF the SH subtropical jet shifts equatorward during El Niño from about 180° to 60°W. In the NH, weak positive (poleward) or insignificant jet shifts with El Niño are seen in DJF and MAM over 180°–120°W. NH subtropical jet latitude shifts with ENSO are insignificant in all seasons over about 60°W–20°E (over the Atlantic). Variations in NH latitude changes in DJF are consistent with the smaller and sometimes insignificant latitude changes in the zonal mean in this season (Fig. 7) and with the weaker DJF anomalies seen in Fig. 3. It is not obvious why the changes in the subtropical jet related to ENSO tend to be weak over the North Atlantic, but we note that this is the region that stands out as having a lower frequency of subtropical jets relative to polar or both polar and subtropical jets in the NH (Fig. 1), so this may be related to the especially complex structures of and mechanisms for variability of the jets in this region. For example, teleconnections from the Madden–Julian oscillation to North Atlantic and European weather regimes depend on the phase of ENSO and have opposite effects during negative and positive phases of the North Atlantic Oscillation, resulting in changes in the Rossby wave activity that drives jet variability that are not directly in concert with ENSO (e.g., Lee et al. 2019). The largest regional subtropical jet latitude shifts (the equatorward shifts during El Niño over the western Pacific

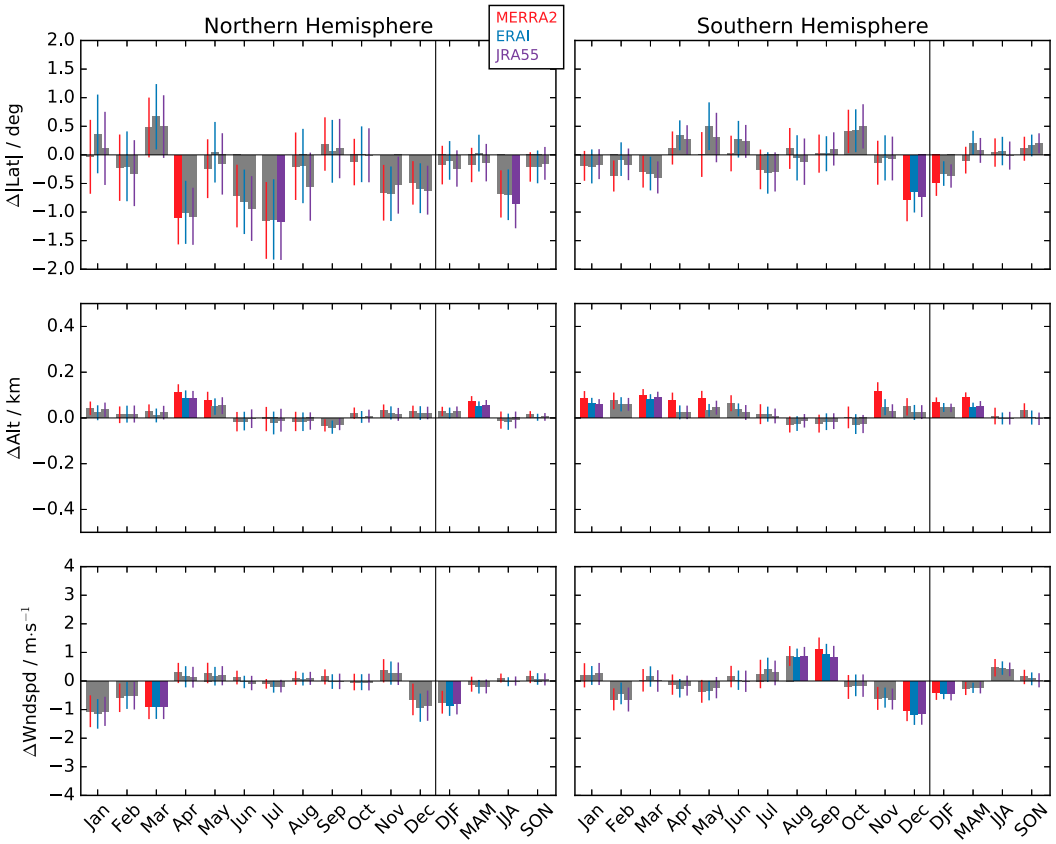


FIG. 8. As in Fig. 7, but for the polar jet.

in both hemispheres) are as much as 3°–4° depending on hemisphere and season.

Significant subtropical jet altitude shifts are always upward during El Niño in both hemispheres, and in some seasons are seen around most of the globe (Fig. 9). In the SH, the largest altitude changes (up to about 0.6 km between weak La Niña and weak El Niño conditions) are over the eastern Pacific and South America from about 180° to 80°W in DJF and MAM. Smaller (but still significant) changes are seen in JJA and SON over the western part of these regions, and in DJF, MAM, and JJA over about 140°–160°E. The largest NH subtropical jet altitude changes (up to about 0.5 km between weak La Niña and weak El Niño conditions) are over the eastern Pacific and North America, with significant changes in DJF around 140°–100°W, in MAM around 140°–40°W, and in JJA and SON around 180°–100°W.

Significant subtropical jet wind speed increases during El Niño (typically from 2 to 6 $m\,s^{-1}$; Fig. 9) are seen over the eastern Pacific and the Americas in DJF and MAM in the NH, and JJA and SON in the SH. Smaller, but still typically significant, wind speed decreases during El Niño are seen from about 180°–120°W in JJA and SON. NH subtropical jet winds are also weaker during El Niño in portions of the 100°E–180° region during DJF, MAM, and SON. In the SH, wind speed decreases with El Niño are significant (although small) in DJF over the eastern Pacific (~160°–100°W) and in JJA and SON over about 20°–120°E.

While there were very few periods with significant correlations of MEIv2 with polar jet characteristics in the zonal mean (Fig. 8), Fig. 10 shows several regions with strong correlations that vary by season. Significant equatorward jet latitude shifts with El Niño (negative values) in the NH occur over East Asia and the western Pacific (around 120°E–180°) in DJF and MAM (with large changes of over 3° in DJF) and over North America (about 120°–140°W) in JJA. The largest SH poleward shifts with El Niño of 2°–3° are seen over the eastern Pacific in JJA and SON. Smaller SH equatorward polar jet shifts during El Niño are seen from about 40°W through the Eastern Hemisphere and across the date line to 160°W; these are significant over most of that region in DJF, and in localized parts of it in JJA and/or SON.

Polar jet altitude changes with ENSO are mostly not significant in either hemisphere in JJA or SON, and where they are their magnitude (change from La Niña to El Niño threshold) is no more than about 0.2 km. In DJF, small but significant upward polar jet shifts during El Niño occur in the NH from about 40°W to 100°E and in the SH from 40° to 80°E and from 120°E across the date line to 160°W. Significant negative changes are seen in the NH in DJF over North America (120°–80°W) and in the SH in JJA and SON in small regions over the eastern Pacific and South America. In MAM, significant upward polar jet shifts during El Niño are seen in the NH from 100°E across the date line to 160°W, and in the SH from 20°E across the date line to 160°W.

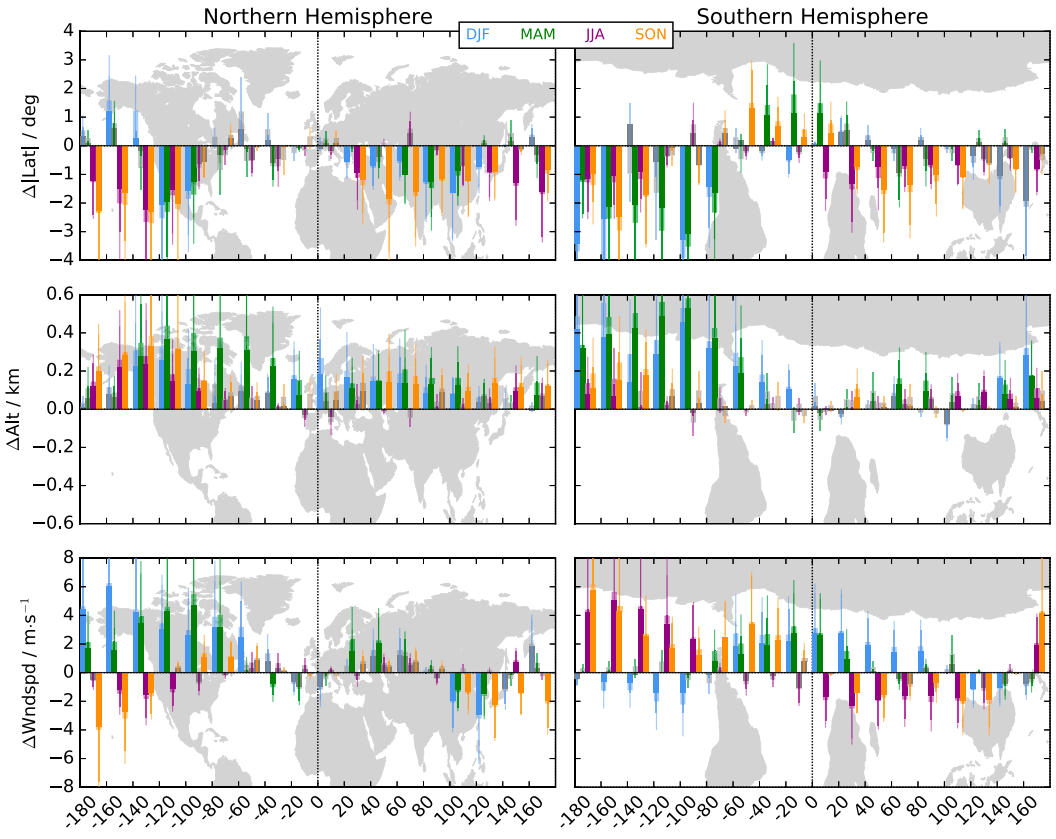


FIG. 9. As in Fig. 7, but for correlations in 20° longitude bins showing largest (transparent colors) and smallest (opaque colors) values among the three reanalyses and color coded by season whenever the correlations are significant at the 95% confidence level. Maps are underlaid to provide a geographical reference and are inverted in the SH as a reminder that we use absolute value of latitude, so a positive latitude shift is always poleward.

Polar jet wind speeds typically weaken during El Niño in the Western Hemisphere and strengthen in the Eastern Hemisphere in both NH and SH, except in the NH in JJA when changes are weak/insignificant everywhere except just east of the Greenwich meridian. These wind speed changes are significant in most of the NH Western Hemisphere in DJF and MAM, and in a smaller region over the eastern Pacific and western North America in SON. In the SH, polar jet wind speed changes are most significant in JJA and SON but still significant in much of the Western Hemisphere in DJF and MAM. The magnitude of significant polar jet wind speed changes is up to 2–3 m $s^{-1}$. The consistent sign change with region in the wind speed variations with ENSO explains the weakness or insignificance of polar jet wind speed changes in the zonal mean, and reflects the Eastern/Western Hemispheric asymmetry seen in the composite maps (Figs. 3–6).

### e. *Discussion/synthesis*

Figure 11 encapsulates the seasonal and regional variations in subtropical and polar jet ENSO-related changes described above, which we summarize and discuss in the following paragraphs.

*Subtropical jet latitude:* Significant subtropical jet latitude changes with MEIV2 are usually negative (equatorward shift during El Niño) in both hemispheres, with the largest changes in DJF and MAM in the SH around 180°–80°W. Our analysis further shows small regions with strong positive changes: in the NH in DJF (~160–120°W) and in the SH in MAM (~20°W–20°E) and SON (~60°–40°W).

*Subtropical jet altitude:* Significant subtropical jet altitude shifts are always positive (upward) during El Niño; the largest upward shifts occur in regions where there are large equatorward latitude shifts during El Niño.

*Subtropical jet wind speed:* Significant changes in subtropical jet wind speed vary in sign, typically showing stronger jets during El Niño over the Western Hemisphere in winter and spring (DJF and MAM in the NH; JJA and SON in the SH). Subtropical jets are weaker during El Niño in the NH surrounding the date line in SON and in the Eastern Hemisphere of the SH in JJA and SON. Thus, in winter and spring in each hemisphere subtropical jet wind speed changes show a "dipole" pattern with opposite signed changes with ENSO in the Western versus Eastern Hemisphere. A similar, but weaker, pattern is seen in SH summer and autumn, but is shifted so that positive changes are over about 60°W through 60°E.

The regional and seasonal subtropical jet correlations summarized above are significant often enough that those signals are reflected in the zonal mean. Substantial negative subtropical jet

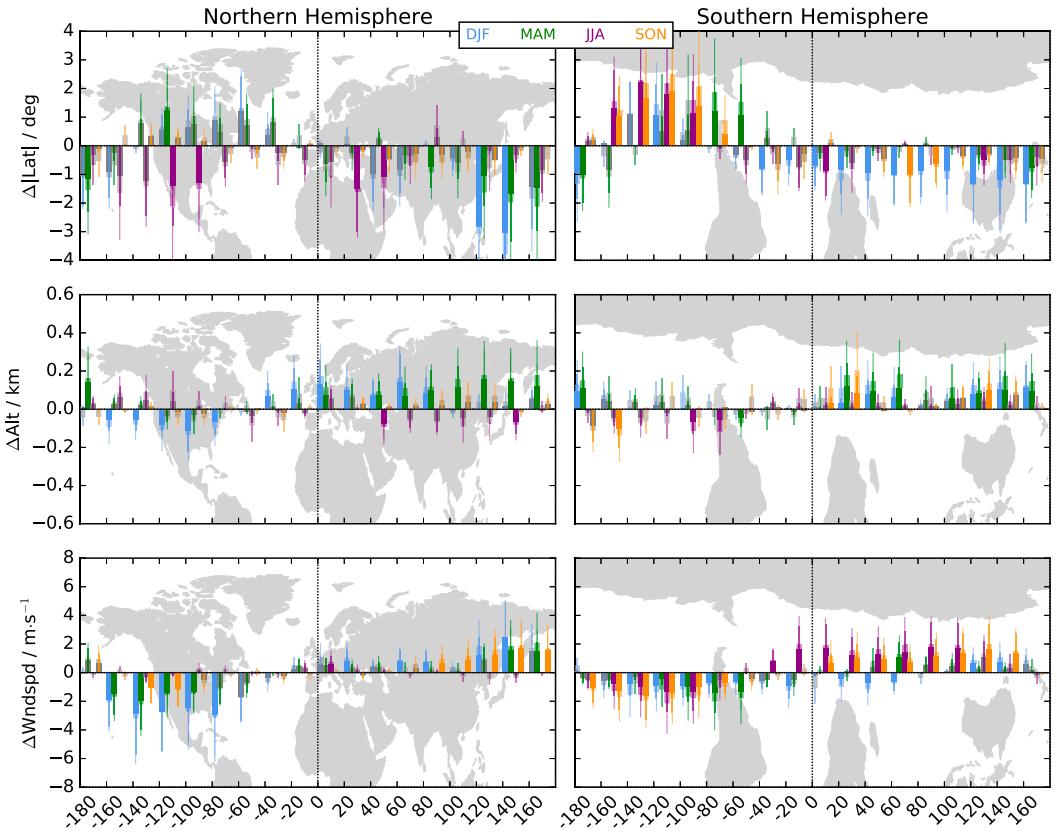


FIG. 10. As in Fig. 9, but for the polar jet.

latitude shifts during El Niño over the Eastern Hemisphere, where the subtropical jet is strongest and most zonal, are consistent with previous work examining shifts in zonal means or broad regions (e.g., Seager et al. 2003; L'Heureux and Thompson 2006; Gillett et al. 2021) and with the qualitative results of Spensberger and Spengler (2020) for all westerly tropopause-level jets. The dipole pattern in subtropical jet wind speeds in SH winter may reflect previously reported opposing Hadley cell behavior in the Eastern and Western Hemispheres (Nguyen et al. 2018). Past studies of jet relationships to ENSO have generally not focused on vertically resolved changes, but our results showing that significant subtropical jet altitude changes are positive during El Niño is consistent with the concurrent latitude shifts and with the climatological anticorrelation between jet latitude and altitude (Fig. S6 in the online supplemental material; e.g., Lorenz and DeWeaver 2007; Hartmann et al. 2013; Manney and Hegglin 2018).

Because of the strong seasonality and regionality of tropical to extratropical teleconnections and the prevalence of indirect pathways for mid-to-high-latitude ENSO influence (Hall et al. 2015; Stan et al. 2017; Domeisen et al. 2019, and references therein), it is not surprising that changes of the polar jets with MEIv2 (Fig. 11, lower panels) are significant less often and over smaller regions than those for the subtropical jets, as summarized below.

*Polar jet latitude:* Equatorward polar jet latitude shifts during El Niño are seen in the NH in DJF and MAM at 120°–160°E and JJA at 120°–80°W, and poleward shifts during El Niño in MAM at 120°–100°W. Significant polar jet latitude changes with ENSO cover larger regions in the SH than in the NH, with SH equatorward shifts with El Niño from 40°E across the date line through 160°W in DJF and poleward shifts in JJA and SON around 160°–80°W.

*Polar jet altitude:* Significant polar jet altitude shifts are usually upward during El Niño, and occur primarily in DJF and MAM, in much of the Eastern Hemisphere in both NH and SH. Significant (although small) downward shifts with El Niño are seen in the NH in DJF over about 160°–60°W, and in the SH in limited portions of the 160°–80°W region in JJA and SON. Most of these downward shifts are coincident with (though not significant in the NH) poleward latitude shifts.

*Polar jet wind speed:* Polar jet wind speeds change with ENSO in a dipole pattern with weaker and stronger jets during El Niño in the Western and Eastern Hemispheres, respectively; these changes are significant over most of the SH except in MAM. Largest changes in the NH are negative over 160°–80°W in DJF and MAM and positive over 120°–160°E in DJF and 80°–180°E in SON.

Previous work related to polar or eddy-driven jet changes with ENSO is difficult to relate to our results because such studies generally identify the polar jet in very different ways. In particular, many such studies define the eddy-driven jet at a

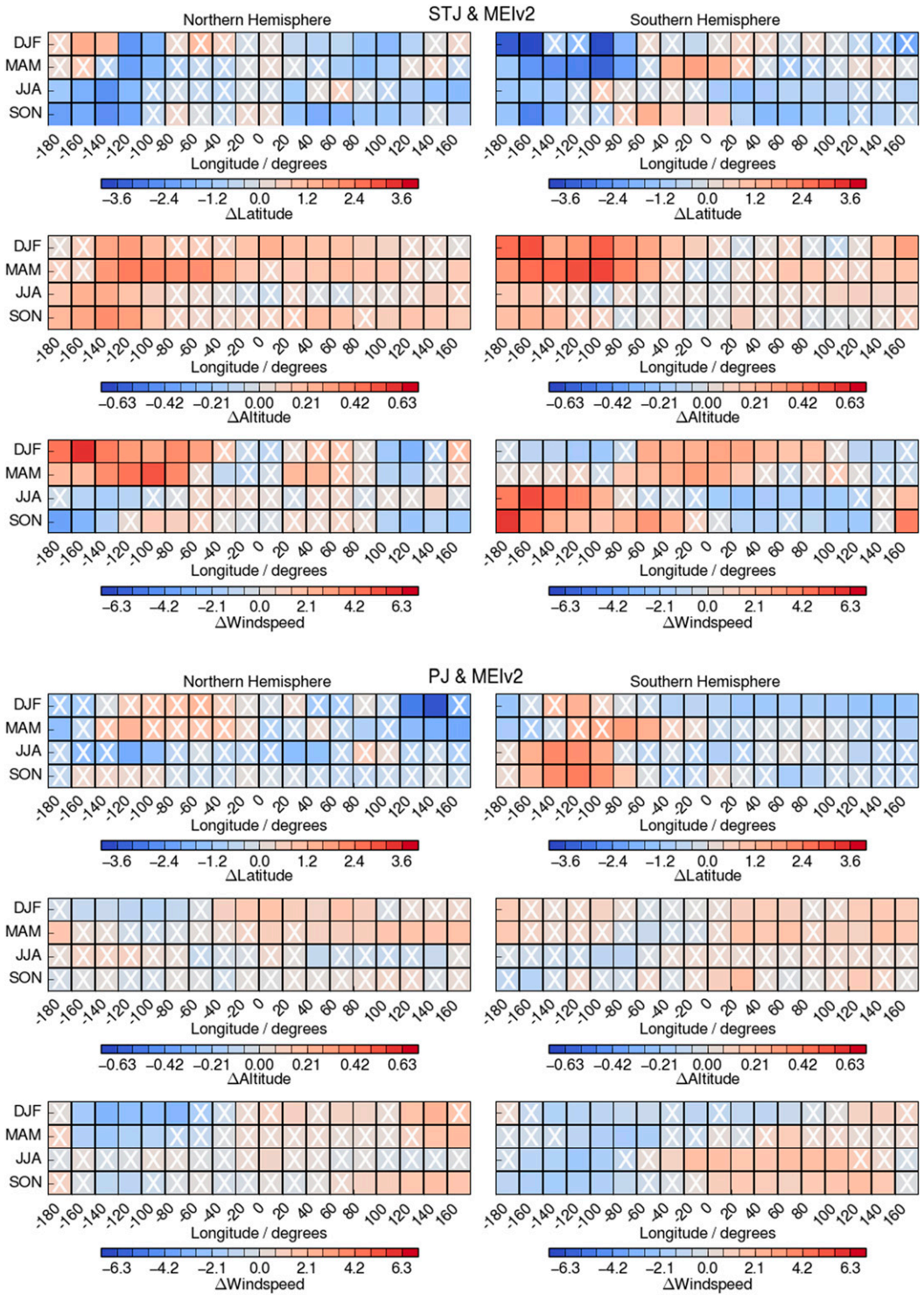


FIG. 11. Summary matrices for (top three rows) subtropical jet and (bottom three rows) polar jet of (top) latitude, (middle) altitude, and (bottom) wind speed change with MEIv2 (within each 3-row block of panels). Color fill shows the value of the change expected if the ENSO state changed from the weakest La Niña to the weakest El Niño. Correlation coefficients for bins with a white X were not significant at the 95% confidence level as based on the bootstrapping analyses. Values are from the reanalysis with the maximum change.

single level using low-level (typically 850 hPa) winds, and usually in zonal means or very broad regions (see, e.g., Gillett et al. 2021, and references therein). This approach is used as a simple way to exclude the subtropical jet since that jet typically does not extend down to 850 hPa (e.g., Woollings et al. 2010, 2014), but it precludes detailed characterization of the full structure and variability of the polar jet such as that done herein.

Where the changes are significant, the magnitudes of ENSO-related changes in latitude, altitude, and wind speed of the polar jet are smaller than those for the subtropical jets. The maximum magnitude of the changes from weak La Niña to weak El Niño conditions for subtropical jets is up to approximately 4°, 0.6 km, and 6 m $s^{-1}$ for latitude, altitude, and wind speed, respectively, and for polar jets is up to approximately 3.5°, 0.3 km, and 3 m $s^{-1}$ for latitude, altitude, and wind speed, respectively.

Because past work has generally focused on zonal mean or broad regions, has generally not looked at ENSO-related changes in three dimensions, and has not used a unified method to consistently define and distinguish the UT subtropical and polar jets, our results provide a unique way to look at concurrent changes of polar and subtropical UT jets. Several regions and seasons show parallel patterns in subtropical and polar ENSO-related jet changes, particularly in wind speed. In winter and spring in both hemispheres, the Eastern/Western Hemisphere dipole pattern of wind speed changes with ENSO has opposite signs for the polar and subtropical jets. This is consistent with the common climatological anticorrelation of subtropical and polar jet wind speeds shown in Fig. 2 (and suggested in previous work, albeit using very different metrics; e.g., Ceppi and Hartmann 2013; Gillett et al. 2021). Such opposing changes tend to reinforce the differences in subtropical versus polar jet wind speeds, so that in the winter hemispheres, subtropical jet wind speeds are even higher relative to polar jet wind speeds during El Niño than they are climatologically (Fig. S10 in the online supplemental material illustrates this situation). While not entirely comparable because of very different jet definitions (although, to the degree that the polar jet is barotropic, reasonable agreement would be expected), this result appears consistent with the aforementioned previous studies. These strong correlations of opposite sign occur in regions and periods when both subtropical and polar jets are typically present (e.g., Fig. 1). They suggest that ENSO influence on the two jets may be linked to differing effects of wave-driving based on the relative strength and position of the two jets, as well as different primary driving mechanisms for the jets. The climatological positive or negative correlation of subtropical or polar jet wind speed, respectively, and latitude (Fig. S6 in the online supplemental material) that was noted in section 2b reflects these differing mechanisms, but the lack of a climatological correlation between subtropical and polar jet latitudes (Fig. 2) argues for the complexity of these relationships. Given past work showing differing effects of wave-driving related to latitude and relative positions of the jets and the differing processes for wave generation and dissipation in the jets (e.g., Lee and Kim 2003; Son and Lee 2005; Eichelberger and Hartmann 2007; Li and Wettstein 2012), as well as evidence that the eddy-driven jet in the lower troposphere weakens as the subtropical jet strengthens during El Niño, examining our results in light of ENSO-related changes in regional patterns of wave-driving should be a fruitful avenue of investigation.

## 4. Conclusions

We have comprehensively characterized the relationships of UT jet stream variability to ENSO. Regional and seasonal jet variations with ENSO are quantified for 1979–2018 using the MEIv2 ENSO index and a daily 3D characterization of the jets. This approach provides a methodologically consistent extension of our work on UT jet climatology and trends (Manney et al. 2014; Manney and Hegglin 2018) and a framework for comprehensively understanding UT jet relationships and linking their variability to driving mechanisms and possible climate impacts. Our results agree closely among the three modern reanalyses used, providing confidence in their robustness. To quantify how extratropical UT jets vary with ENSO, we characterized subtropical and polar jets separately and analyzed their regional and seasonal variability in relation to the MEIv2 index.

Evaluation of maps and cross sections of El Niño/La Niña differences in UT jet occurrence frequency and wind speed shows strong seasonal, regional, and hemispheric variability in the relationships of UT jets to ENSO. The tropical jets (both easterly and westerly) associated with monsoon and Walker circulations are stronger during La Niña than during El Niño, consistent with previous studies showing strengthening of tropical circulations during La Niña (Julian and Chervin 1978; Horinouchi et al. 2000; Waugh and Polvani 2000; Bayr et al. 2014, and references therein). Manney and Hegglin (2018) noted that an increasing trend in the equatorial jets associated with the Walker circulation and the Australian monsoon in DJF was consistent with a greater prevalence of La Niña conditions in recent boreal winters. The patterns of anomalies in extratropical westerly jets reported herein are consistent with the qualitative patterns shown by Spensberger and Spengler (2020) for all westerly UT jets.

Correlations of ENSO with subtropical jet variations are sufficiently consistent across large regions that most seasons show significant correlations in the zonal mean: The subtropical jet latitude shifts equatorward with El Niño and poleward with La Niña, except in DJF in the NH and MAM in the SH. Subtropical jet altitudes increase during El Niño in the NH and in DJF and MAM in the SH. Subtropical jet wind speeds show significant increases during El Niño in the NH in DJF and MAM and in the SH in MAM and SON. The NH shows a significant decrease in subtropical jet wind speed in SON. Despite prevalent equatorward shifts of the subtropical jets during El Niño, small regions do show strong poleward shifts in the NH in DJF and in the SH in MAM and SON. Subtropical jet trends are commonly less robust than this ENSO-related variability, but Manney and Hegglin (2018) showed a poleward trend in DJF over Africa and Asia that appears consistent with more La Niña–like conditions in recent years in that season.

In contrast, and consistent with less direct pathways for ENSO influence on the polar jets, ENSO/polar jets correlations are usually not significant in the zonal mean. However, regional/seasonal polar jet correlations show equatorward NH polar jet latitude shifts during El Niño in localized regions of the NH in DJF, MAM, and JJA, and localized poleward shifts

during El Niño in MAM. In the SH there are significant equatorward polar jet shifts during El Niño throughout the Eastern Hemisphere in DJF, and poleward polar jet shifts during El Niño over much of the Western Hemisphere in JJA and SON. The polar jet shifts upward during El Niño in both hemispheres in many regions in DJF and MAM but shifts downward in much of the NH Western Hemisphere in DJF.

Regional wintertime subtropical jet wind speeds in both NH and SH are often higher in the Western Hemisphere and lower in the Eastern Hemisphere during El Niño. Conversely, polar jet wind speed changes in both NH and SH are characterized by weaker jets in the Western Hemisphere and stronger jets in the Eastern Hemisphere during El Niño, especially in winter and spring. This dipole pattern of ENSO-related wind speed changes occurs in regions and seasons when both subtropical and polar jets are typically present. Along with the climatological anticorrelation between subtropical and polar jet wind speeds (which reinforces these changes), this result indicates ENSO-related covariability of the subtropical and polar jets. Future work is planned to link these changes with ENSO-related variations in forcing of the jets.

This work provides a uniquely comprehensive analysis of the relationships of interannual variability in UT subtropical and polar jet streams to ENSO and highlights the importance and complexity of seasonal and regional variability in those relationships. Because of the important roles both the UT jets and ENSO play in shaping weather and climate, this information and future related studies will continue to increase our understanding of these atmospheric processes. In particular, we plan to conduct similar analyses of climate and subseasonal-to-seasonal forecast model simulations to assess how well models capture these relationships and how this information can help us predict future relationships.

*Acknowledgments.* We thank the Microwave Limb Sounder team at the Jet Propulsion Laboratory, especially Brian Knosp and Luis Millán, for computational, data processing, management, and analysis support; Mark Olsen, Ted Shepherd, Isla Simpson, and three anonymous reviewers for helpful discussions and/or comments; and NASA's GMAO, ECMWF, and JMA for providing their assimilated data products. Authors Manney and Lawrence were partially supported by the JPL Microwave Limb Sounder team under a JPL subcontract, under NASA Grant NNX14AE85G, and under NSF Climate and Large-scale Dynamics Grant 2015906.

*Data availability statement.* The datasets used are publicly available online, as follows: MERRA-2 (https://disc.sci.gsfc.nasa.gov/uui/datasets?keywords=%22MERRA-2%22), ERA-I (http://apps.ecmwf.int/datasets/), JRA-55 (through NCAR RDA; https://doi.org/10.5065/D6HH6H41) and MEIv2 indices (https://www.esrl.noaa.gov/psd/enso/mei/).

## REFERENCES

Bai, K., N.-B. Chang, and W. Gao, 2016: Quantification of relative contribution of Antarctic ozone depletion to increased austral extratropical precipitation during 1979–2013. *J. Geophys. Res. Atmos.*, **121**, 1459–1474, https://doi.org/10.1002/2015JD024247.

Bayr, T., D. Dommenget, T. Martin, and S. B. Power, 2014: The eastward shift of the Walker circulation in response to global warming and its relationship to ENSO variability. *Climate Dyn.*, **43**, 2747–2763, https://doi.org/10.1007/s00382-014-2091-y.

Bloom, S. C., L. L. Takacs, A. M. da Silva, and D. Ledvina, 1996: Data assimilation using incremental analysis updates. *Mon. Wea. Rev.*, **124**, 1256–1271, https://doi.org/10.1175/1520-0493(1996)124<1256:DAUIAU>2.0.CO;2.

Bollasina, M. A., Y. Ming, V. Ramaswamy, M. D. Schwarzkopf, and V. Naik, 2014: Contribution of local and remote anthropogenic aerosols to the twentieth century weakening of the South Asian monsoon. *Geophys. Res. Lett.*, **41**, 680–687, https://doi.org/10.1002/2013GL058183.

Byrne, N. J., T. G. Shepherd, T. Woollings, and R. A. Plumb, 2017: Nonstationarity in Southern Hemisphere climate variability associated with the seasonal breakdown of the stratospheric polar vortex. *J. Climate*, **30**, 7125–7139, https://doi.org/10.1175/JCLI-D-17-0097.1.

——, ——, and I. Polichtchouk, 2019: Subseasonal-to-seasonal predictability of the Southern Hemisphere eddy-driven jet during austral spring and early summer. *J. Geophys. Res. Atmos.*, **124**, 6841–6855, https://doi.org/10.1029/2018JD030173.

Calvo, N., R. R. Garcia, W. J. Randel, and D. R. Marsh, 2010: Dynamical mechanism for the increase in tropical upwelling in the lowermost tropical stratosphere during warm ENSO events. *J. Atmos. Sci.*, **67**, 2331–2340, https://doi.org/10.1175/2010JAS3433.1.

Ceppi, P., and D. L. Hartmann, 2013: On the speed of the eddy-driven jet and the width of the Hadley cell in the Southern Hemisphere. *J. Climate*, **26**, 3450–3465, https://doi.org/10.1175/JCLI-D-12-00414.1.

Chen, G., and I. M. Held, 2007: Phase speed spectra and the recent poleward shift of Southern Hemisphere surface westerlies. *Geophys. Res. Lett.*, **34**, L21805, https://doi.org/10.1029/2007GL031200.

——, J. Lu, and D. M. W. Frierson, 2008: Phase speed spectra and the latitude of surface westerlies: Interannual variability and global warming trend. *J. Climate*, **21**, 5942–5959, https://doi.org/10.1175/2008JCLI2306.1.

Dee, D. P., and Coauthors, 2011: The ERA-Interim reanalysis: Configuration and performance of the data assimilation system. *Quart. J. Roy. Meteor. Soc.*, **137**, 553–597, https://doi.org/10.1002/qj.828.

Delworth, T. L., and F. Zeng, 2014: Regional rainfall decline in Australia attributed to anthropogenic greenhouse gases and ozone levels. *Nat. Geosci.*, **7**, 583–587, https://doi.org/10.1038/ngeo2201.

Domeisen, D. I., C. I. Garfinkel, and A. H. Butler, 2019: The teleconnection of El Niño Southern Oscillation to the stratosphere. *Rev. Geophys.*, **57**, 5–47, https://doi.org/10.1029/2018RG000596.

Ebita, A., and Coauthors, 2011: The Japanese 55-year Reanalysis "JRA-55": An interim report. *SOLA*, **7**, 149–152, https://doi.org/10.2151/sola.2011-038.

Eichelberger, S. J., and D. L. Hartmann, 2007: Zonal jet structure and the leading mode of variability. *J. Climate*, **20**, 5149–5163, https://doi.org/10.1175/JCLI4279.1.

Efron, B., and R. J. Tibshirani, 1993: *An Introduction to the Bootstrap*. Chapman and Hall, 452 pp.

Fujiwara, M., and Coauthors, 2017: Introduction to the SPARC Reanalysis Intercomparison Project (S-RIP) and overview of the reanalysis systems. *Atmos. Chem. Phys.*, **17**, 1417–1452, https://doi.org/10.5194/acp-17-1417-2017.

Garfinkel, C. I., and D. L. Hartmann, 2008: Different ENSO teleconnections and their effects on the stratospheric polar vortex. *J. Geophys. Res.*, **113**, D18114, https://doi.org/10.1029/2008JD009920.

Gelaro, R., and Coauthors, 2017: The Modern-Era Retrospective Analysis for Research and Applications, version-2 (MERRA-2). *J. Climate*, **30**, 5419–5454, https://doi.org/10.1175/JCLI-D-16-0758.1.

Gillett, Z. E., H. H. Hendon, J. M. Arblaster, and E.-P. Lim, 2021: Tropical and extratropical influences on the variability of the Southern Hemisphere wintertime subtropical jet. *J. Climate*, **34**, 4009–4022, https://doi.org/10.1175/JCLI-D-20-0460.1.

GMAO, 2015: MERRA-2 inst3_3d_asm_Nv: 3D, 3-hourly, instantaneous, model-level, assimilation, assimilated meteorological fields v5.12.4, Goddard Earth Sciences Data and Information Services Center (GES DISC), accessed 1 November 2015, https://doi.org/10.5067/WWQSXQ8IVFW8.

Grise, K. M., S. M. Davis, P. W. Staten, and O. Adam, 2018: Regional and seasonal characteristics of the recent expansion of the tropics. *J. Climate*, **31**, 6839–6856, https://doi.org/10.1175/JCLI-D-18-0060.1.

Grotjahn, R., and Coauthors, 2016: North American extreme temperature events and related large scale meteorological patterns: A review of statistical methods, dynamics, modeling, and trends. *Climate Dyn.*, **46**, 1151–1184, https://doi.org/10.1007/s00382-015-2638-6.

Hall, R., R. Erdélyi, E. Hanna, J. M. Jones, and A. A. Scaife, 2015: Drivers of North Atlantic Polar Front jet stream variability. *Int. J. Climatol.*, **35**, 1697–1720, https://doi.org/10.1002/joc.4121.

Harnik, N., C. I. Garfinkel, and O. Lachmy, 2016: The influence of jet stream regime on extreme weather events. *Dynamics and Predictability of Large-Scale, High-Impact Weather and Climate Events*, J. Li, Ed., Cambridge University Press, 79–94, https://doi.org/10.1017/CBO9781107775541.007.

Hartmann, D. L., 2015: Pacific sea surface temperature and the winter of 2014. *Geophys. Res. Lett.*, **42**, 1894–1902, https://doi.org/10.1002/2015GL063083.

——, and Coauthors, 2013: Observations: Atmosphere and surface. *Climate Change 2013: The Physical Science Basis*, T. F. Stocker et al., Eds., Cambridge University Press, 159–254.

Held, I. M., M. Ting, and H. Wang, 2002: Northern winter stationary waves: Theory and modeling. *J. Climate*, **15**, 2125–2144, https://doi.org/10.1175/1520-0442(2002)015<2125:NWSWTA>2.0.CO;2.

Homeyer, C. R., and Coauthors, 2021: Extratropical upper troposphere and lower stratosphere (ExUTLS). Chapter 7, SPARC Reanalysis Intercomparison Project (S-RIP) Final Report, SPARC Report No. 10, WCRP-6/2021, 263–306, https://www.sparc-climate.org/wp-content/uploads/sites/5/2021/07/07_SRIP_Report_Ch07_EarlyOnlineRelease.pdf; https://doi.org/10.17874/800dee57d13, in press.

Horinouchi, T., F. Sassi, and B. A. Boville, 2000: Synoptic-scale Rossby waves and the geographic distribution of lateral transport routes between the tropics and the extratropics in the lower stratosphere. *J. Geophys. Res.*, **105**, 26 579–26 592, https://doi.org/10.1029/2000JD900281.

Huang, D.-Q., J. Zhu, Y.-C. Zhang, J. Wang, and X.-Y. Kuang, 2015: The impact of the East Asian subtropical jet and polar front jet on the frequency of spring persistent rainfall over Southern China in 1997–2011. *J. Climate*, **28**, 6054–6066, https://doi.org/10.1175/JCLI-D-14-00641.1.

Hudson, R. D., 2012: Measurements of the movement of the jet streams at mid-latitudes, in the Northern and Southern Hemispheres, 1979 to 2010. *Atmos. Chem. Phys.*, **12**, 7797–7808, https://doi.org/10.5194/acp-12-7797-2012.

Hulme, M., and N. Tosdevin, 1989: The tropical easterly jet and Sudan rainfall: A review. *Theor. Appl. Climatol.*, **39**, 179–187, https://doi.org/10.1007/BF00867945.

Julian, P., and R. Chervin, 1978: A study of the Southern Oscillation and Walker circulation phenomenon. *Mon. Wea. Rev.*, **106**, 1433–1451, https://doi.org/10.1175/1520-0493(1978)106<1433:ASOTSO>2.0.CO;2.

Kang, S. M., L. M. Polvani, J. C. Fyfe, and M. Sigmond, 2011: Impact of polar ozone depletion on subtropical precipitation. *Science*, **332**, 951–954, https://doi.org/10.1126/science.1202131.

Kelly, P., L. R. Leung, K. Balaguru, W. Xu, B. Mapes, and B. Soden, 2018: Shape of Atlantic tropical cyclone tracks and the Indian monsoon. *Geophys. Res. Lett.*, **45**, 10 746–10 755, https://doi.org/10.1029/2018GL080098.

Kobayashi, S., and Coauthors, 2015: The JRA-55 reanalysis: General specification and basic characteristics. *J. Meteor. Soc. Japan*, **93**, 5–48, https://doi.org/10.2151/jmsj.2015-001.

Kolstad, E. W., T. Breiteig, and A. A. Scaife, 2010: The association between stratospheric weak polar vortex events and cold air outbreaks in the Northern Hemisphere. *Quart. J. Roy. Meteor. Soc.*, **136**, 886–893, https://doi.org/10.1002/qj.620.

Lee, R. W., S. J. Woolnough, A. J. Charlton-Perez, and F. Vitart, 2019: ENSO modulation of MJO teleconnections to the North Atlantic and Europe. *Geophys. Res. Lett.*, **46**, 13 535–13 545, https://doi.org/10.1029/2019GL084683.

Lee, S., and H.-K. Kim, 2003: The dynamical relationship between subtropical and eddy-driven jets. *J. Atmos. Sci.*, **60**, 1490–1503, https://doi.org/10.1175/1520-0469(2003)060<1490:TDRBSA>2.0.CO;2.

L'Heureux, M. L., and D. W. J. Thompson, 2006: Observed relationships between the El Niño–Southern Oscillation and the extratropical zonal-mean circulation. *J. Climate*, **19**, 276–287, https://doi.org/10.1175/JCLI3617.1.

Li, C., and J. J. Wettstein, 2012: Thermally driven and eddy-driven jet variability in reanalysis. *J. Climate*, **25**, 1587–1596, https://doi.org/10.1175/JCLI-D-11-00145.1.

Lin, M., L. W. Horowitz, S. J. Oltmans, A. M. Fiore, and S. Fan, 2014: Tropospheric ozone trends at Mauna Loa Observatory tied to decadal climate variability. *Nat. Geosci.*, **7**, 136–143, https://doi.org/10.1038/ngeo2066.

——, A. M. Fiore, L. W. Horowitz, A. O. Langford, S. J. Oltmans, D. Tarasick, and H. E. Rieder, 2015: Climate variability modulates western US ozone air quality in spring via deep stratospheric intrusions. *Nat. Commun.*, **6**, 7105, https://doi.org/10.1038/ncomms8105.

Long, C. S., M. Fujiwara, S. Davis, D. M. Mitchell, and C. J. Wright, 2017: Climatology and interannual variability of dynamic variables in multiple reanalyses evaluated by the SPARC Reanalysis Intercomparison Project (S-RIP). *Atmos. Chem. Phys.*, **17**, 14 593–14 629, https://doi.org/10.5194/acp-17-14593-2017.

Lorenz, D. J., and E. T. DeWeaver, 2007: Tropopause height and zonal wind response to global warming in the IPCC scenario integrations. *J. Geophys. Res.*, **112**, D10119, https://doi.org/10.1029/2006JD008087.

Lucas, C., and H. Nguyen, 2015: Regional characteristics of tropical expansion and the role of climate variability. *J. Geophys. Res. Atmos.*, **120**, 6809–6824, https://doi.org/10.1002/2015JD023130.

——, ——, and B. Timbal, 2012: An observational analysis of Southern Hemisphere tropical expansion. *J. Geophys. Res.*, **117**, D17112, https://doi.org/10.1029/2011JD017033.

——, B. Timbal, and H. Nguyen, 2014: The expanding tropics: A critical assessment of the observational and modeling studies. *Wiley Interdiscip. Rev.: Climate Change*, **5**, 89–112, https://doi.org/10.1002/wcc.251.

Maher, P., M. E. Kelleher, P. G. Sansom, and J. Methven, 2020: Is the subtropical jet shifting poleward? *Climate Dyn.*, **54**, 1741–1759, https://doi.org/10.1007/s00382-019-05084-6.

Mann, M. E., S. Rahmstorf, K. Kornhuber, B. A. Steinman, S. K. Miller, and D. Coumou, 2017: Influence of anthropogenic climate change on planetary wave resonance and extreme weather events. *Sci. Rep.*, **7**, 45242, https://doi.org/10.1038/srep45242.

Manney, G. L., and M. I. Hegglin, 2018: Seasonal and regional variations in long-term changes in upper tropospheric jets from reanalyses. *J. Climate*, **31**, 423–448, https://doi.org/10.1175/JCLI-D-17-0303.1.

——, and Coauthors, 2011: Jet characterization in the upper troposphere/lower stratosphere (UTLS): Applications to climatology and transport studies. *Atmos. Chem. Phys.*, **11**, 6115–6137, https://doi.org/10.5194/acp-11-6115-2011.

——, M. I. Hegglin, W. H. Daffer, M. J. Schwartz, M. L. Santee, and S. Pawson, 2014: Climatology of upper tropospheric–lower stratospheric (UTLS) jets and tropopauses in MERRA. *J. Climate*, **27**, 3248–3271, https://doi.org/10.1175/JCLI-D-13-00243.1.

——, and Coauthors, 2017: Reanalysis comparisons of upper tropospheric–lower stratospheric jets and multiple tropopauses. *Atmos. Chem. Phys.*, **17**, 11 541–11 566, https://doi.org/10.5194/acp-17-11541-2017.

——, M. L. Santee, Z. D. Lawrence, K. Wargan, and M. J. Schwartz, 2021: A moments view of climatology and variability of the Asian summer monsoon anticyclone. *J. Climate*, **34**, 7821–7841, https://doi.org/10.1175/JCLI-D-20-0729.1.

Martineau, P., H. Nakamura, and Y. Kosaka, 2021: Influence of ENSO on North American subseasonal surface air temperature variability. *Wea. Climate Dyn.*, **2**, 395–412, https://doi.org/10.5194/wcd-2-395-2021.

McLandress, C., T. G. Shepherd, J. F. Scinocca, D. A. Plummer, M. Sigmond, A. I. Jonsson, and M. C. Reader, 2011: Separating the dynamical effects of climate change and ozone depletion. Part II: Southern Hemisphere troposphere. *J. Climate*, **24**, 1850–1868, https://doi.org/10.1175/2010JCLI3958.1.

Melamed-Turkish, K., P. A. Taylor, and J. Liu, 2018: Upper-level winds over eastern North America: A regional jet stream climatology. *Int. J. Climatol.*, **38**, 4740–4757, https://doi.org/10.1002/joc.5693.

Nakamura, H., T. Sampe, Y. Tanimoto, and A. Shimpo, 2004: Observed associations among storm tracks, jet streams and midlatitude oceanic fronts. *Earth's Climate: The Ocean–Atmosphere Interaction*, *Geophys. Monogr.*, Vol. 147, Amer. Geophys. Union, 329–345, https://doi.org/10.1029/147GM18.

Nguyen, H., H. H. Hendon, E. P. Lim, G. Boschat, E. Maloney, and B. Timbal, 2018: Variability of the extent of the Hadley circulation in the Southern Hemisphere: A regional perspective. *Climate Dyn.*, **50**, 129–142, https://doi.org/10.1007/s00382-017-3592-2.

Peña-Ortiz, C., D. Gallego, P. Ribera, P. Ordonez, and M. D. C. Alvarez-Castro, 2013: Observed trends in the global jet stream characteristics during the second half of the 20th century. *J. Geophys. Res. Atmos.*, **118**, 2702–2713, https://doi.org/10.1002/jgrd.50305.

Politis, D. N., and J. P. Romano, 1994: The stationary bootstrap. *J. Amer. Stat. Assoc.*, **89**, 1303–1313, https://doi.org/10.1080/01621459.1994.10476870.

Price, C., L. Stone, A. Huppert, B. Rajagopalan, and P. Alpert, 1998: A possible link between El Niño and precipitation in Israel. *Geophys. Res. Lett.*, **25**, 3963–3966, https://doi.org/10.1029/1998GL900098.

Raible, C. C., U. Luksch, and K. Fraedrich, 2004: Precipitation and Northern Hemisphere regimes. *Atmos. Sci. Lett.*, **5**, 43–55, https://doi.org/10.1016/j.atmoscilet.2003.12.001.

RavindraBabu, S., M. Venkat Ratnam, G. Basha, and B. V. Krishnamurthy, 2019: Indian summer monsoon onset signatures on the tropical tropopause layer. *Atmos. Sci. Lett.*, **20**, e884, https://doi.org/10.1002/asl.884.

Santos, J. A., T. Woollings, and J. G. Pinto, 2013: Are the winters 2010 and 2012 archetypes exhibiting extreme opposite behavior of the North Atlantic jet stream? *Mon. Wea. Rev.*, **141**, 3626–3640, https://doi.org/10.1175/MWR-D-13-00024.1.

Scaife, A. A., C. K. Folland, L. V. Alexander, A. Moberg, and J. R. Knight, 2008: European climate extremes and the North Atlantic Oscillation. *J. Climate*, **21**, 72–83, https://doi.org/10.1175/2007JCLI1631.1.

Schiemann, R., D. Lüthi, and C. Schar, 2009: Seasonality and interannual variability of the westerly jet in the Tibetan Plateau region. *J. Climate*, **22**, 2940–2957, https://doi.org/10.1175/2008JCLI2625.1.

Schubert, S., H. Wang, and M. Suarez, 2011: Warm season subseasonal variability and climate extremes in the Northern Hemisphere: The role of stationary Rossby waves. *J. Climate*, **24**, 4773–4792, https://doi.org/10.1175/JCLI-D-10-05035.1.

Seager, R., N. Harnik, Y. Kushnir, W. Robinson, and J. Miller, 2003: Mechanisms of hemispherically symmetric climate variability. *J. Climate*, **16**, 2960–2978, https://doi.org/10.1175/1520-0442(2003)016<2960:MOHSCV>2.0.CO;2.

Shaman, J., and E. Tziperman, 2007: Summertime ENSO–North African–Asian jet teleconnection and implications for the Indian monsoons. *Geophys. Res. Lett.*, **34**, L11702, https://doi.org/10.1029/2006GL029143.

Shapiro, M. A., H. Wernli, N. A. Bond, and R. Langland, 2001: The influence of the 1997–99 El Niño Southern Oscillation on extratropical baroclinic life cycles over the eastern North Pacific. *Quart. J. Roy. Meteor. Soc.*, **127**, 331–342, https://doi.org.10.1002/qj.49712757205.

Son, S. W., and S. Lee, 2005: The response of westerly jets to thermal driving in a primitive equation model. *J. Atmos. Sci.*, **62**, 3741–3757, https://doi.org/10.1175/JAS3571.1.

Spensberger, C., and T. Spengler, 2020: Feature-based jet variability in the upper troposphere. *J. Climate*, **33**, 6849–6871, https://doi.org/10.1175/JCLI-D-19-0715.1.

Stan, C., D. M. Straus, J. S. Frederiksen, H. Lin, E. D. Maloney, and C. Schumacher, 2017: Review of tropical–extratropical teleconnections on intraseasonal time scales. *Rev. Geophys.*, **55**, 902–937, https://doi.org/10.1002/2016RG000538.

Staten, P. W., K. M. Grise, and S. M. Davis, 2016: The width of the tropics: Climate variations and their impacts. *SPARC Newsletter*, No. 46, 26–31.

Strong, C., and R. E. Davis, 2007: Winter jet stream trends over the Northern Hemisphere. *Quart. J. Roy. Meteor. Soc.*, **133**, 2109–2115, https://doi.org/10.1002/qj.171.

——, and ——, 2008: Variability in the position and strength of winter jet stream cores related to Northern Hemisphere teleconnections. *J. Climate*, **21**, 584–592, https://doi.org/10.1175/2007JCLI1723.1.

Tanaka, H., N. Ishizaki, and A. Kitoh, 2004: Trend and interannual variability of Walker, monsoon, and Hadley circulations defined by velocity potential in the upper troposphere. *Tellus*, **56A**, 250–269, https://doi.org/10.3402/tellusa.v56i3.14410.

Tegtmeier, S., and Coauthors, 2020: Temperature and tropopause characteristics from reanalyses data in the tropical tropopause layer. *Atmos. Chem. Phys.*, **20**, 753–770, https://doi.org/10.5194/acp-20-753-2020.

——, and Coauthors, 2021: Tropical troposphere layer. Chapter 8, SPARC Reanalysis Intercomparison Project (S-RIP) Final

Report, SPARC Report No. 10, WCRP-6/2021, 307–388, https://www.sparc-climate.org/wp-content/uploads/sites/5/2021/07/08_SRIP_Report_Ch08_EarlyOnlineRelease-2.pdf; https://doi.org/10.17874/800dee57d13, in press.

Thompson, D. W., S. Solomon, P. J. Kushner, M. H. Grise, and D. J. Karoly, 2011: Signatures of the Antarctic ozone hole in Southern Hemisphere surface climate change. *Nat. Geosci.*, **4**, 741–749, https://doi.org/10.1038/ngeo1296.

Uccellini, L. W., and D. R. Johnson, 1979: The coupling of upper and lower tropospheric jet streaks and implications for the development of severe convective storms. *Mon. Wea. Rev.*, **107**, 682–703, https://doi.org/10.1175/1520-0493(1979)107<0682:TCOUAL>2.0.CO;2.

Wang, S.-Y., L. Hipps, R. R. Gillies, and J.-H. Yoon, 2014: Probable causes of the abnormal ridge accompanying the 2013–2014 California drought: ENSO precursor and anthropogenic warming footprint. *Geophys. Res. Lett.*, **41**, 3220–3226, https://doi.org/10.1002/2014GL059748.

Waugh, D. W., and L. M. Polvani, 2000: Climatology of intrusions into the tropical upper troposphere. *Geophys. Res. Lett.*, **27**, 3857–3860, https://doi.org/10.1029/2000GL012250.

——, C. I. Garfinkel, and L. M. Polvani, 2015: Drivers of the recent tropical expansion in the Southern Hemisphere: Changing SSTs or ozone depletion? *J. Climate*, **28**, 6581–6586, https://doi.org/10.1175/JCLI-D-15-0138.1.

——, and Coauthors, 2018: Revisiting the relationship among metrics of tropical expansion. *J. Climate*, **31**, 7565–7581, https://doi.org/10.1175/JCLI-D-18-0108.1.

Wettstein, J. J., and J. M. Wallace, 2010: Observed patterns of month-to-month storm-track variability and their relationship to the background flow. *J. Atmos. Sci.*, **67**, 1420–1437, https://doi.org/10.1175/2009JAS3194.1.

Wilks, D. S., 2011: *Statistical Methods in the Atmospheric Sciences*. 3rd ed. Elsevier, 676 pp.

Williams, L. N., S. Lee, and S.-W. Son, 2007: Dynamics of the Southern Hemisphere spiral jet. *J. Atmos. Sci.*, **64**, 548–563, https://doi.org/10.1175/JAS3939.1.

Winters, A. C., L. F. Bosart, and D. Keyser, 2019: Antecedent North Pacific jet regimes conducive to the development of continental U.S. extreme temperature events during the cool season. *Wea. Forecasting*, **34**, 393–414, https://doi.org/10.1175/WAF-D-18-0168.1.

Wolter, K., and M. S. Timlin, 2011: El Niño/Southern Oscillation behaviour since 1871 as diagnosed in an extended multivariate ENSO index (MEI.ext). *Int. J. Climatol.*, **31**, 1074–1087, https://doi.org/10.1002/joc.2336.

Woollings, T., A. Hannachi, and B. Hoskins, 2010: Variability of the North Atlantic eddy-driven jet stream. *Quart. J. Roy. Meteor. Soc.*, **136**, 856–868, https://doi.org/10.1002/qj.625.

——, C. Czuchnicki, and C. Franzke, 2014: Twentieth century North Atlantic jet variability. *Quart. J. Roy. Meteor. Soc.*, **140**, 783–791, https://doi.org/10.1002/qj.2197.

——, and Coauthors, 2018: Daily to decadal modulation of jet variability. *J. Climate*, **31**, 1297–1314, https://doi.org/10.1175/JCLI-D-17-0286.1.

Wright, J. S., and Coauthors, 2020: Differences in tropical high clouds among reanalyses: Origins and radiative impacts. *Atmos. Chem. Phys.*, **20**, 8989–9030, https://doi.org/10.5194/acp-20-8989-2020.

Xian, T., and C. R. Homeyer, 2019: Global tropopause altitudes in radiosondes and reanalyses. *Atmos. Chem. Phys.*, **19**, 5661–5678, https://doi.org/10.5194/acp-19-5661-2019.

Xie, Z., Y. Du, and S. Yang, 2015: Zonal extension and retraction of the subtropical westerly jet stream and evolution of precipitation over East Asia and the western Pacific. *J. Climate*, **28**, 6783–6798, https://doi.org/10.1175/JCLI-D-14-00649.1.

Yu, B., and X. Zhang, 2015: A physical analysis of the severe 2013/2014 cold winter in North America. *J. Geophys. Res. Atmos.*, **120**, 10 149–10 165, https://doi.org/10.1002/2015JD023116.

Yulaeva, E., and J. M. Wallace, 1994: The signature of ENSO in global temperature and precipitation fields derived from the Microwave Sounding Unit. *J. Climate*, **7**, 1719–1736, https://doi.org/10.1175/1520-0442(1994)007<1719:TSOEIG>2.0.CO;2.

Zhang, K., T. Wang, M. Xu, and J. Zhang, 2019: Influence of wintertime polar vortex variation on the climate over the North Pacific during late winter and spring. *Atmosphere*, **10**, 670, https://doi.org/10.3390/atmos10110670.

Zhang, T., A. Hoell, J. Perlwitz, J. Eischeid, D. Murray, M. Hoerling, and T. M. Hamill, 2019: Towards probabilistic multivariate ENSO monitoring. *Geophys. Res. Lett.*, **46**, 10 532–10 540, https://doi.org/10.1029/2019GL083946.

Zhao, Y., X. Yu, J. Yao, and X. Dong, 2018: Evaluation of the subtropical westerly jet and its effects on the projected summer rainfall over central Asia using multi-CMIP5 models. *Int. J. Climatol.*, **38** (Suppl.), e1176–e1189, https://doi.org/10.1002/joc.5443.